

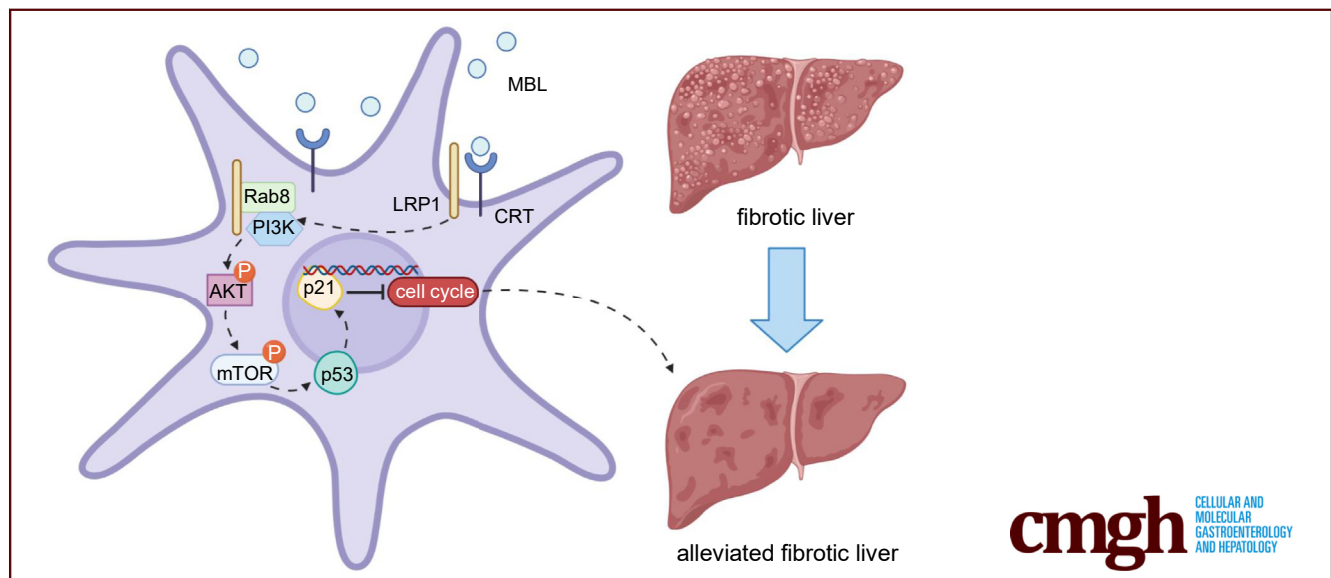
## ORIGINAL RESEARCH

## Mannan-Binding Lectin via Interaction With Cell Surface Calreticulin Promotes Senescence of Activated Hepatic Stellate Cells to Limit Liver Fibrosis Progression



Jialiang Luo,<sup>1,2</sup> Lei Li,<sup>1,2</sup> Bo Chang,<sup>1</sup> Zhengyumeng Zhu,<sup>1,2</sup> Fan Deng,<sup>1,2</sup> Mengyao Hu,<sup>1</sup> Yu Yu,<sup>1</sup> Xiao Lu,<sup>1</sup> Zhengliang Chen,<sup>1</sup> Daming Zuo,<sup>2</sup> and Jia Zhou<sup>1</sup>

<sup>1</sup>Department of Immunology, School of Basic Medical Sciences, <sup>2</sup>Department of Medical Laboratory, School of Laboratory Medicine and Biotechnology, Southern Medical University, Guangzhou, Guangdong, China



## SUMMARY

Mannan-binding lectin is a crucial component in the liver microenvironment. Here, we discovered that mannan-binding lectin–hepatic stellate cell interaction via cell surface calreticulin promotes senescence of activated hepatic stellate cells, contributing to the control of hepatic fibrosis progression.

**BACKGROUND & AIMS:** Liver fibrosis represents a hallmark of most chronic liver diseases (CLD) triggered by recurrent liver injury and subsequent myofibroblast transdifferentiations of resident hepatic stellate cells (HSCs). Mannan-binding lectin (MBL) is potentially involved in hepatic fibrosis in CLD through unclear mechanisms. Therefore, we investigated the crosstalk between MBL and HSCs, and the consequent effects on fibrosis progression.

**METHODS:** Samples from patients with liver cirrhosis were collected. MBL deficiency (MBL<sup>-/-</sup>) and wild-type (WT) C57BL/6J mice were used to construct a CCl<sub>4</sub>-induced liver fibrosis model. Administration of MBL-expressing, liver-specific, adeno-associated virus was performed to restore hepatic MBL

expression in MBL<sup>-/-</sup> mice. The human HSC line LX-2 was used for in vitro experiments.

**RESULTS:** MBL levels in patients with liver cirrhosis were correlated with disease severity. In the CCl<sub>4</sub>-induced liver fibrosis model, MBL<sup>-/-</sup> mice showed severer liver fibrosis accompanied by reduced senescent activated HSCs in liver tissue compared with WT mice, which could be inhibited by administering MBL-expressing, liver-specific, adeno-associated virus. Moreover, depleting senescent cells with senolytic treatment could abrogate these differences owing to MBL absence. Furthermore, MBL could interact directly with calreticulin associated with low-density lipoprotein receptor-related protein 1 on the cell surface of HSCs, which further promotes senescence in HSCs by up-regulating the mammalian target of rapamycin/p53/p21 signaling pathway.

**CONCLUSIONS:** MBL as a newfound senescence-promoting modulator and its crosstalk with HSCs in the liver microenvironment is essential for the control of hepatic fibrosis progression, suggesting its potential therapeutic use in treating CLD associated with liver fibrosis. (*Cell Mol Gastroenterol Hepatol* 2022;14:75–99; <https://doi.org/10.1016/j.jcmgh.2022.03.011>)

**Keywords:** Mannan-Binding Lectin; Hepatic Stellate Cell Senescence; Liver Fibrosis.

Hepatic fibrogenesis results from a repeated wound-healing response to chronic injuries and subsequent accumulation of excessive extracellular matrix (ECM) that progressively deteriorates liver structure and function.<sup>1</sup> Without proper and prompt treatment, liver fibrosis, as a common pathologic process of most chronic liver diseases (CLDs), can progress into cirrhosis, carcinoma, and liver failure, becoming one of the major public health problems worldwide.<sup>2</sup> Of note, the onset and progression of hepatic fibrosis and its regression process are orchestrated by the integrated network consisting of numerous molecules and cells with profibrotic or antifibrotic function in the local environment, among which hepatic stellate cells (HSCs) are a key piece of the puzzle.<sup>3</sup>

Upon liver fibrosis induction, liver injuries and inflammation trigger the activation of HSCs, leading to the trans-differentiation of quiescent, vitamin A-storing HSCs into ECM-secreting, fibrogenic myofibroblasts that now are well established as a central driver of fibrosis.<sup>4</sup> Recent discoveries have shown that activated HSCs with a senescent phenotype might help control and/or reverse liver fibrosis by reducing ECM levels, thus reestablishing the quiescent environment.<sup>5,6</sup> Therefore, how activated HSCs restore the quiescent state through cellular senescence needs to be elucidated, contributing to the development of effective therapies for the treatment of hepatic fibrosis.<sup>7</sup> Although the fate of activated HSCs is regulated by an interdependent network of molecular and cellular components in the liver microenvironment,<sup>8,9</sup> the underlying mechanisms of HSC senescence induction are still unclear.

Mannan (or mannose)-binding lectin (MBL), which belongs to the family of collectins, is a soluble pattern recognition molecule produced primarily by hepatocytes.<sup>10-12</sup> MBL can mediate phagocytosis and trigger the complement cascade through the lectin pathway by binding to carbohydrate motifs.<sup>13</sup> In human beings, the MBL genetic system comprises 1 functional gene (*MBL2*) that encoded MBL2, whereas rodents have 2 MBL isomers (*Mbl1* and *Mbl2*) that encode MBL-A and MBL-C, respectively.<sup>12</sup> In addition, the single human MBL gene is closely related to rodent *Mbl2* rather than rodent *Mbl1*.<sup>14</sup> Moreover, we previously showed the prevalence of MBL-C expression but not MBL-A in the liver of wild-type (WT) mice.<sup>15</sup> Therefore, we focused on the MBL-C (mice) and *MBL2* (human) and used MBL to indicate both of them in the present study. In addition, MBL could exert different biologic functions apart from complement activation, playing crucial roles in tissue homeostasis and various diseases.<sup>10,16,17</sup> Emerging evidence has indicated that MBL is involved in the development of fibrosis in CLD patients, including patients with liver cirrhosis,<sup>18</sup> hepatitis C virus patients with more severe fibrosis,<sup>19</sup> individuals with schistosomiasis-induced liver fibrosis,<sup>20</sup> and patients with HBV-related liver cirrhosis.<sup>21</sup> Our previous study showed that MBL, as an essential component of the liver microenvironment, suppresses

tumor development via interaction with local stromal cells.<sup>15</sup> However, the exact function of MBL in liver fibrosis, especially its crosstalk with other cells in the local environment and the consequent effects on fibrosis progression, has not yet been thoroughly investigated.


In this study, we found a notable association between MBL level and severity of liver fibrosis in human beings. Then, we used a mouse model of CCl<sub>4</sub>-induced liver fibrosis in MBL-deficient mice and human HSC cell line LX-2, seeking to elucidate the potential role of MBL in liver fibrosis and its underlying mechanisms. Our findings uncovered a previously unrecognized mechanism in which MBL-HSC interaction promoted HSC senescence and subsequent fibrosis alleviation, providing insight into a therapeutic strategy for CLD associated with liver fibrosis.

## Results

### *MBL Levels Are Increased During Liver Fibrosis and Associated Inversely With Cirrhosis Severity*

Because MBL is reportedly involved in hepatic fibrosis,<sup>18</sup> we decided to address the association of MBL and liver fibrosis progression. Examination of the plasma MBL concentration in patients with liver cirrhosis and healthy controls using enzyme linked immunosorbent assay (ELISA) analysis showed that MBL levels were markedly higher in cirrhosis patients (Figure 1A). Then, we assessed the association between plasma MBL levels and clinical characteristics in these patients. The correlation analysis showed that cirrhosis patients with higher plasma alanine aminotransferase (ALT) and aspartate aminotransferase (AST) activity tend to display lower MBL levels in plasma, indicating their inverse correlations (Figure 1B-E). Plasma MBL levels in these patients also were correlated inversely with Child-Pugh grade (Figure 1F), whereas levels were associated positively with the plasma concentrations of albumin (Figure 1B). In addition, we observed significantly lower MBL expression and fewer MBL-positive cells in the liver tissue of patients with Child-Pugh B liver cirrhosis than those with Child-Pugh A liver cirrhosis by immunohistochemical staining (Figure 1G). Consistently, in an established murine model of CCl<sub>4</sub>-induced liver fibrosis, the level of MBL protein (Figure 1H and I) and its messenger RNA (mRNA) expression (Figure 1J) were increased in the liver

**Abbreviations used in this paper:**  $\alpha$ -SMA,  $\alpha$ -smooth muscle actin; ALT, alanine aminotransferase; AST, aspartate aminotransferase; CRT, calreticulin; CLD, chronic liver diseases; D, dasatinib; ECM, extracellular matrix; ELISA, enzyme-linked immunosorbent assay; HRP, horseradish peroxidase; HSC, hepatic stellate cell; LDH, lactate dehydrogenase; LRP1, low-density lipoprotein receptor-related protein 1; MBL, mannan-binding lectin; mRNA, messenger RNA; mTOR, mammalian target of rapamycin; pAAV-MBL, mannan-binding lectin-expressing adeno-associated virus; PCR, polymerase chain reaction; PFT- $\alpha$ , pifithrin- $\alpha$ ; PI3K, phosphatidylinositol-3-kinase; Q, quercetin; SA- $\beta$ -Gal, senescence-associated- $\beta$ -galactosidase; WT, wild-type.

 Most current article

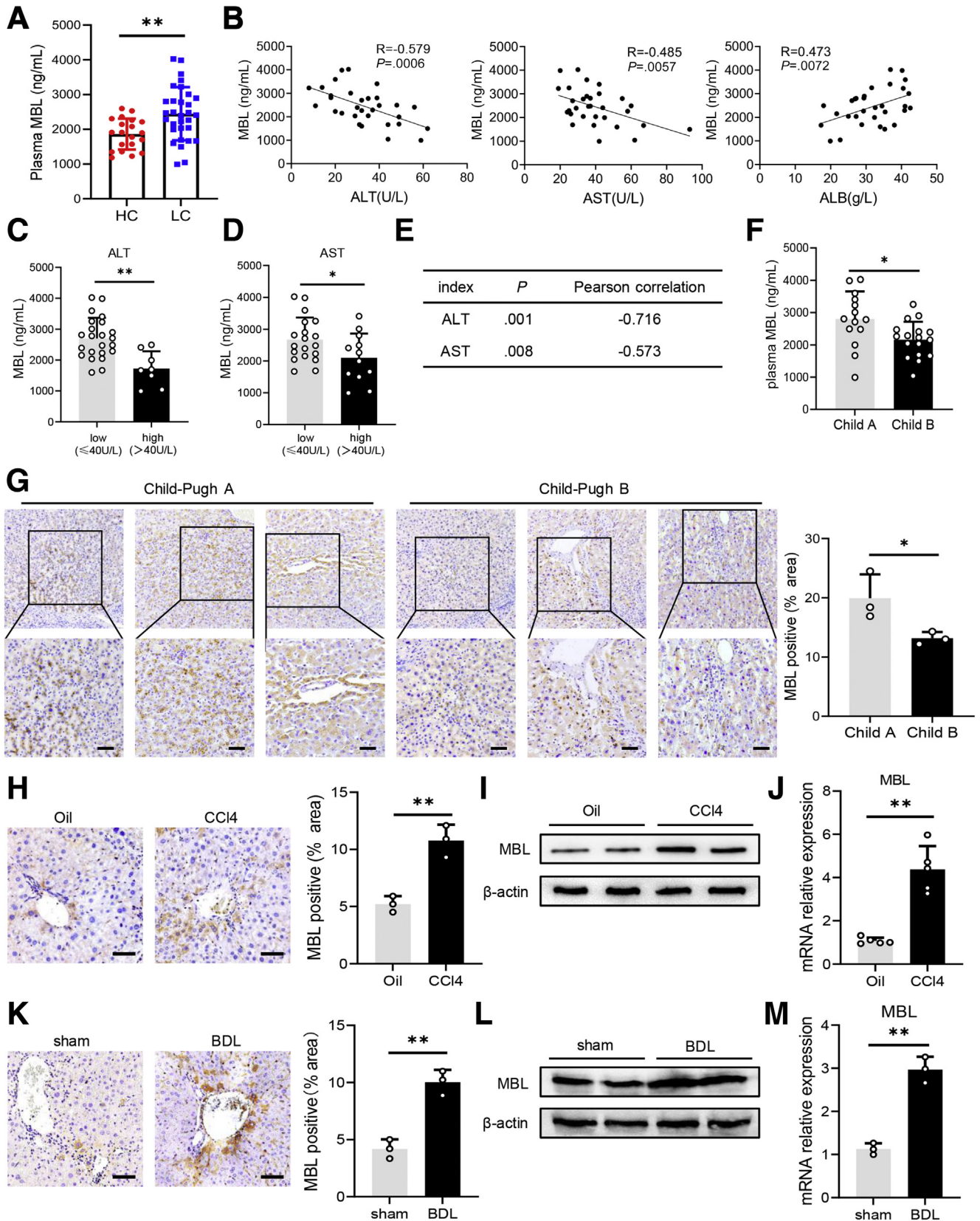
© 2022 The Authors. Published by Elsevier Inc. on behalf of the AGA Institute. This is an open access article under the CC BY-NC-ND license (<http://creativecommons.org/licenses/by-nc-nd/4.0/>).

2352-345X

<https://doi.org/10.1016/j.jcmgh.2022.03.011>

upon fibrogenesis. We observed that MBL distributes throughout the liver and is seen predominantly around the central vein and sinusoid (Figure 1H). Similar results also

were observed in the bile duct ligation model of liver fibrosis (Figure 1K-M). Therefore, these data suggest that MBL is involved in the progression of hepatic fibrosis.



### MBL Contributes to Control of Liver Fibrosis Progression

Because MBL might have a potential role in the pathogenesis of hepatic fibrosis, we further address the exact role of MBL in the ongoing development of liver fibrosis. First, we used MBL<sup>-/-</sup> mice and WT littermates to investigate the characteristics of liver fibrosis in the CCl<sub>4</sub>-induced murine model. We observed that ALT and AST levels and lactate dehydrogenase (LDH) activity in serum from MBL<sup>-/-</sup> mice markedly increased compared with those from WT mice after CCl<sub>4</sub> treatment (Figure 2A). The histologic staining of liver sections showed that CCl<sub>4</sub>-treated MBL<sup>-/-</sup> mice displayed a larger fibrosis area in liver tissue than WT counterparts (Figure 2B). Furthermore, Sirius Red staining (Figure 2C) and Masson's trichrome staining (Figure 2D), respectively, showed significantly more collagen deposition and fibrous connective tissue hyperplasia in liver tissue of MBL<sup>-/-</sup> mice compared with that of WT controls. Because liver fibrosis also is characterized by activated HSCs in which  $\alpha$ -smooth muscle actin ( $\alpha$ -SMA) is a vital indicator,<sup>22</sup> we subsequently assessed  $\alpha$ -SMA levels in the liver. As expected, the expression of  $\alpha$ -SMA in liver sections (Figure 2E), as well as intrahepatic  $\alpha$ -SMA protein (Figure 2F) and its mRNA expression (Figure 2G), strongly increased in MBL<sup>-/-</sup> mice compared with those in WT mice upon CCl<sub>4</sub>-induced fibrogenesis. The quantitative reverse-transcription polymerase chain reaction (PCR) results showed that the mRNA levels of fibrosis-associated genes remarkably increased in isolated HSCs of MBL<sup>-/-</sup> mice compared with those of WT controls during liver fibrosis (Figure 2H). These results indicate that MBL absence led to a deterioration of liver fibrosis.

Furthermore, we subsequently performed a tail-vein administration of liver-specific MBL-expressing, adeno-associated virus (pAAV-MBL) to restore MBL expression in the liver of MBL-deficient mice as we reported previously,<sup>15</sup> followed by CCl<sub>4</sub> injection and further assessment of liver fibrosis. Immunohistochemistry and Western blot analysis in the liver tissue showed that MBL<sup>-/-</sup> mice lack MBL expression, while MBL expression was restored after pAAV-MBL injection (Figure 3A and B). Consistently, much more fibrous connective tissue hyperplasia and collagen deposition in liver tissue were observed in MBL<sup>-/-</sup> mice than in WT counterparts, as determined by histologic staining (Figure 3C). Similar to the earlier-described results in mice without pAAV administration, MBL<sup>-/-</sup> mice with pAAV-

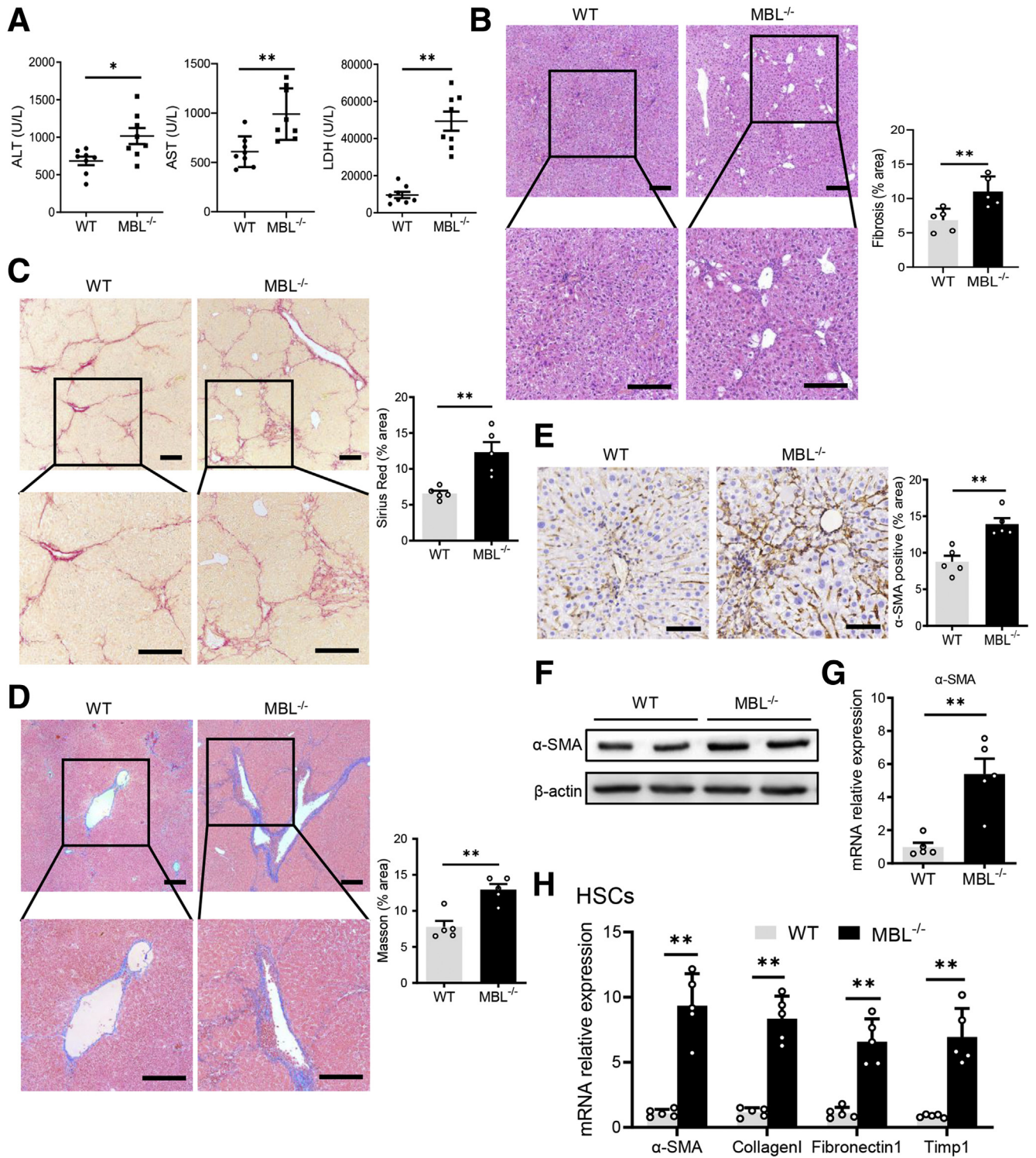
control pretreatment showed markedly increased intrahepatic  $\alpha$ -SMA expression (Figure 3C). However, pAAV-MBL delivery nearly eliminated the progression of liver fibrosis owing to the absence of MBL, indicated by comparable liver fibrosis features in WT mice and MBL<sup>-/-</sup> mice (Figure 3C and D). Collectively, these data showed that restoration of hepatic MBL expression relieves the liver fibrosis progression owing to MBL deficiency, implying that MBL contributed to the amelioration of liver fibrosis progression.

### MBL Limits Liver Fibrosis Progression via Promoting HSC Senescence

During hepatic fibrosis, some activated HSCs might progressively undergo senescence, becoming less fibrogenic, thus holding a vital position in controlling fibrosis.<sup>23</sup> Together with the earlier-described results that determined the MBL involvement in the control of hepatic fibrosis, emerging data raised a potential association between MBL and activated HSC senescence in liver fibrosis. Interestingly, as shown in the senescence-associated- $\beta$ -galactosidase (SA- $\beta$ -Gal) staining that indicated the senescent cells,<sup>24</sup> the number of SA- $\beta$ -Gal<sup>+</sup> cells decreased dramatically in liver sections of MBL<sup>-/-</sup> mice compared with that of WT mice (Figure 4A). In addition, MBL deficiency strikingly increased the proliferative Ki67<sup>+</sup> cells in liver tissue, as determined by immunohistochemistry staining (Figure 4B). Moreover, we investigated that p21, as one of the cellular senescence markers, was expressed by  $\alpha$ -SMA<sup>+</sup> activated HSCs in fibrotic liver sections, and the p21<sup>+</sup> $\alpha$ -SMA<sup>+</sup> cell frequency notably decreased as a result of MBL deficiency (Figure 4C). In accordance with the histologic staining, the mRNA expression of senescence-related genes, including senescence-associated secretory phenotype genes, decreased significantly in isolated HSCs of MBL<sup>-/-</sup> mice compared with those of WT controls (Figure 4D). Moreover, hepatic MBL restoration through liver-specific pAAV-MBL delivery in MBL<sup>-/-</sup> mice eliminated the reduction of the senescent activated HSC cell frequency (Figure 5A) and the protein (p53 and p21) expression of senescence-related genes as well as their mRNA levels owing to the absence of MBL (Figure 5B and C). These results indicated that MBL expression led to an amelioration of liver fibrosis progression along with the increased frequency of senescent activated HSCs.

Senescent cells can be selectively eliminated by dasatinib and quercetin (D+Q) administration, which belongs to a

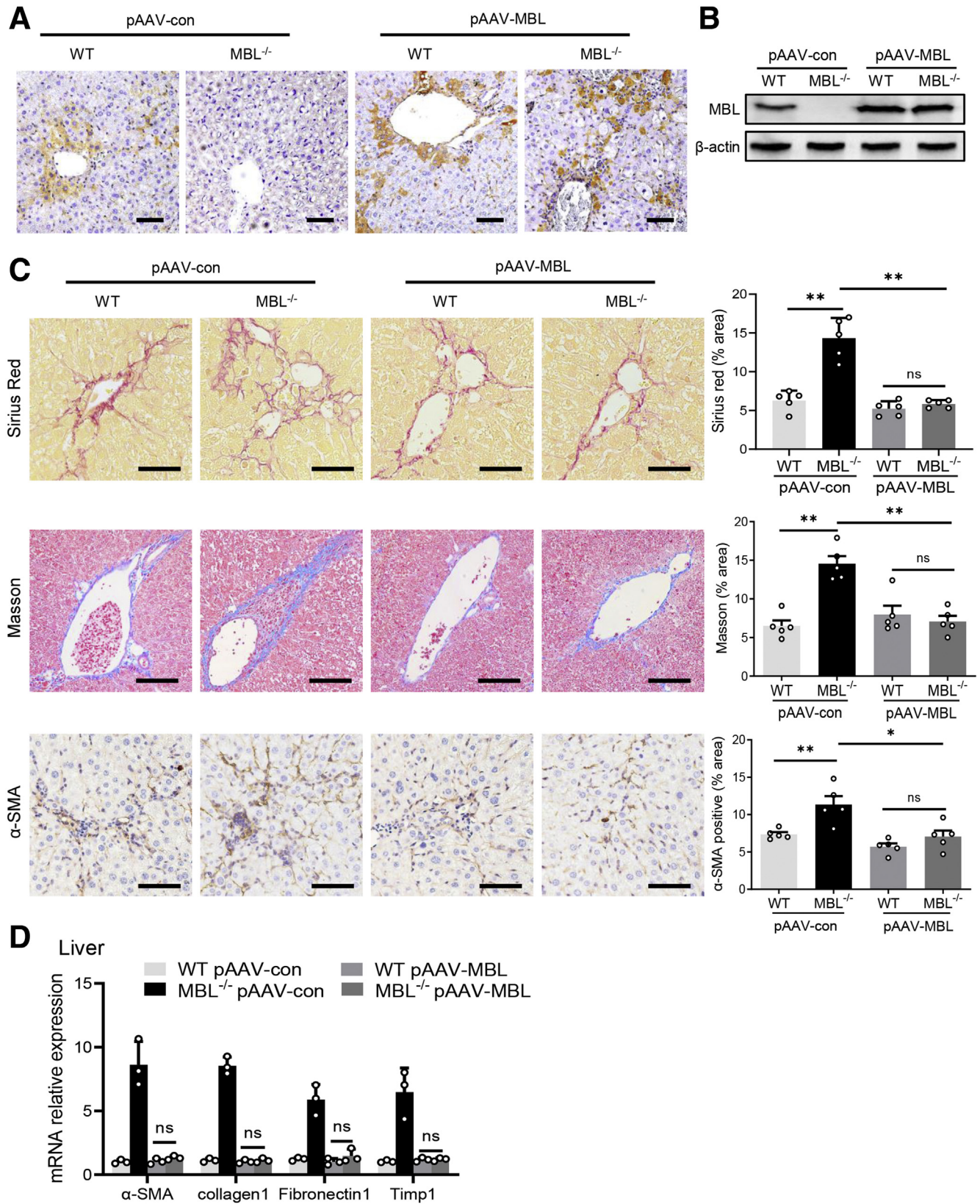
**Figure 1. (See previous page). MBL levels increase during liver fibrosis and are associated negatively with cirrhosis severity.** (A) The concentration of the serum MBL in healthy volunteers (n = 20) and liver cirrhotic patients (n = 31) was determined by ELISA. (B) The relationship between plasma MBL concentration and AST, ALT, and albumin levels in liver cirrhotic patients. (C) The concentration of MBL in liver cirrhosis patients with high ALT and low ALT levels. (D) The concentration of MBL in liver cirrhosis patients with high AST and low AST levels. (E) The correlation of MBL and AST, and ALT in cirrhosis patients. (F) Quantification of serum MBL concentration in liver cirrhosis patients with Child-Pugh A and Child-Pugh B. (G) Representative images and statistical analysis of MBL expression in liver sections from liver cirrhosis patients with Child-Pugh A (n = 3) and Child-Pugh B (n = 3). Mice (n = 5 per group) were injected with oil or CCl<sub>4</sub> for 6 weeks. (H) Representative photomicrographs of MBL staining in mouse livers. The (I) protein levels and (J) mRNA levels of MBL were assessed by Western blot and quantitative reverse-transcription (qRT)-PCR analysis, respectively. Mice (n = 5 per group) were subjected to BDL model for 3 weeks. (K) The protein levels of MBL in liver tissues of WT and MBL<sup>-/-</sup> mice. The (L) protein levels and (M) mRNA levels of MBL were assessed by Western blot and qRT-PCR analysis, respectively. Scale bars: 100  $\mu$ m. Data are presented as means  $\pm$  SEM. \**P* < .05, \*\**P* < .01, Student *t* test. HC, healthy control; LC, liver cirrhosis.



**Figure 2. MBL deficiency aggravates liver fibrosis.** MBL<sup>-/-</sup> and WT mice (n = 8 per group) were injected with CCl<sub>4</sub> for 6 weeks. (A) The serum concentration of ALT, AST, and LDH. (B) Representative photomicrographs of H&E staining in livers of WT and MBL<sup>-/-</sup> mice with the establishment of liver fibrosis. Representative photomicrographs of (C) Sirius Red and (D) Masson's trichrome staining in fibrotic livers of WT and MBL<sup>-/-</sup> mice. The (E) immunohistochemical staining, (F) protein expression, and (G) mRNA levels of α-SMA in liver tissues. (H) The quantitative reverse-transcription PCR analysis of mRNA levels of fibrosis-related genes in primary HSCs from WT and MBL<sup>-/-</sup> mice. Scale bars: 100 μm. Data are presented as means ± SEM. \*P < .05, \*\*P < .01, Student t test. Timp1, tissue inhibitors of metalloproteinase 1.

new class of drugs known as “senolytics.”<sup>25</sup> Recently, although there are no efficient drugs to selectively target senescent HSCs, D+Q, as the most prominent senolytic,

shows toxicity toward senescent HSCs and thus can be used to deplete senescent HSCs in the liver.<sup>26</sup> To testify whether the senescent HSCs are involved in MBL-mediated



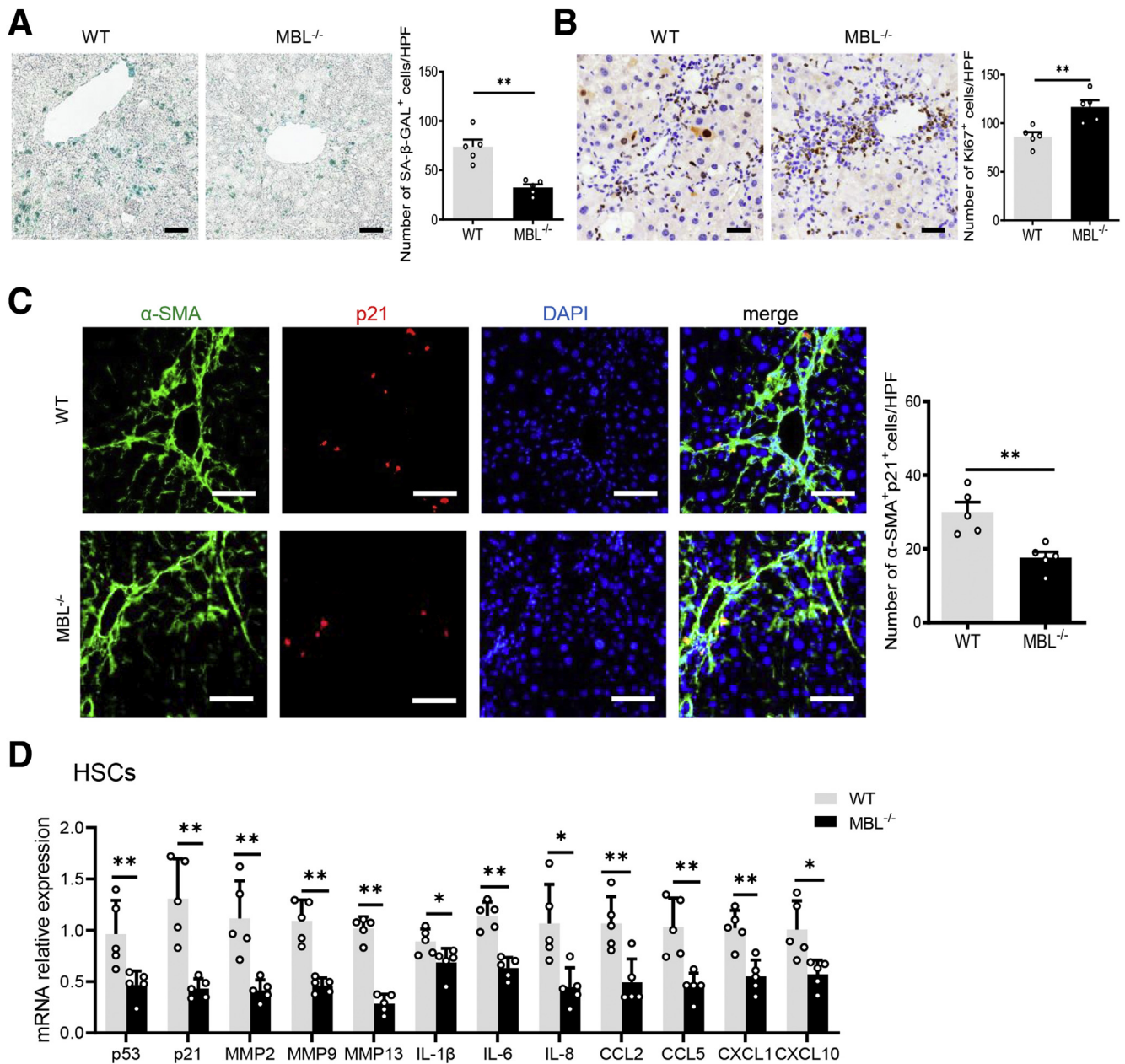
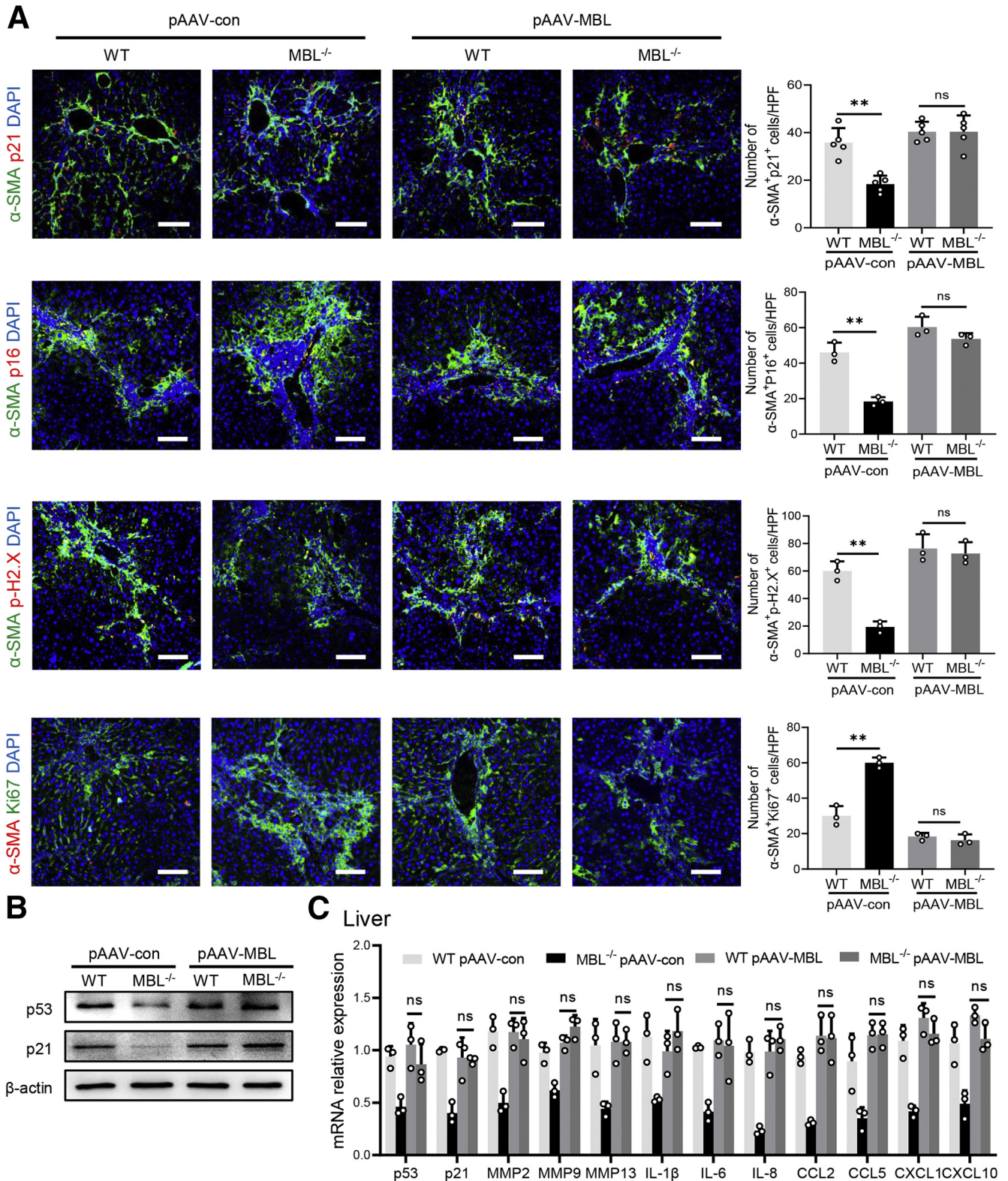


**Figure 4. MBL deficiency leads to decreased frequency of senescent HSCs.** The MBL<sup>-/-</sup> and WT mice (n = 8 per group) were injected with CCl<sub>4</sub> for 6 weeks. Representative photomicrographs of (A) SA-β-gal staining and (B) Ki67 staining in fibrotic livers of WT and MBL<sup>-/-</sup> mice. Scale bars: 100 μm. (C) Representative immunofluorescence staining of α-SMA (green) and p21 (red) in liver tissues of WT and MBL<sup>-/-</sup> mice. Scale bars: 50 μm. (D) The mRNA levels of senescence-related genes in primary HSCs of CCl<sub>4</sub>-treated WT and MBL<sup>-/-</sup> mice. Data are presented as means ± SEM. \*P < .05, \*\*P < .01, Student *t* test. CCL, chemokine (C-C motif) ligand; CXCL, chemokine (C-X-C motif) ligand; DAPI, 4',6-diamidino-2-phenylindole; HPF, high-power field; IL, interleukin; MMP, matrix metalloproteinase.

**Figure 3. (See previous page). AAV-mediated restoration of hepatic MBL expression abrogates the deterioration of liver fibrosis as a result of MBL deficiency.** The MBL<sup>-/-</sup> and WT mice (n = 5 per group) received a pAAV-control or pAAV-MBL vector injection 3 weeks before liver fibrosis establishment. (A) Representative photomicrographs of MBL histologic staining in the liver tissues of WT and MBL<sup>-/-</sup> mice injected with pAAV-control or pAAV-MBL vectors. (B) The protein levels of MBL in liver tissues were assessed by Western blot analysis. (C) Representative photomicrographs of Sirius Red, Masson's trichrome, and α-SMA histologic staining in the liver tissues. (D) The mRNA levels of fibrosis-related genes in livers were assessed by quantitative reverse-transcription PCR analysis. Scale bars: 100 μm. Data are presented as means ± SEM. \*\*P < .01, 1-way analysis of variance followed by Tukey post hoc tests for multiple group comparisons. Timp1, tissue inhibitors of metalloproteinase 1.





amelioration of liver fibrosis progression, we applied senolytic drugs (D+Q) by oral administration along with CCl<sub>4</sub> administration to eliminate senescent HSCs in WT mice. To evaluate the eliminating effect of senolytic drugs on senescent cells in liver, we performed co-staining of  $\alpha$ -SMA and other cellular senescent indicators or Ki67 in liver sections. The results show that D+Q treatment significantly reduced the frequency of senescent activated HSCs, whereas it increased the number of Ki67<sup>+</sup> $\alpha$ -SMA<sup>+</sup> cells (Figure 6A). In addition, co-staining of  $\alpha$ -SMA and pro-apoptosis molecule Bax or anti-apoptosis protein Bcl2 showed that D+Q treatment increased the frequency of  $\alpha$ -SMA<sup>+</sup>Bax<sup>+</sup> cells while reducing the presence of  $\alpha$ -SMA<sup>+</sup>Bcl2<sup>+</sup> cells, whereas they became comparable between WT and MBL<sup>-/-</sup> mice (Figure 6B). In addition, the protein expression (p53 and p21) and mRNA levels of representative senescence-related genes including senescence-associated secretory phenotype genes in liver tissues were reduced after senolytic administration (Figure 6C and D). Furthermore, WT mice showed notably more liver injury, fibrous connective tissue hyperplasia, and collagen deposition in liver sections after D+Q treatment, which was comparable with D+Q-treated MBL<sup>-/-</sup> mice (Figure 7). Taken together, these results suggest that HSC senescence might be responsible for MBL-mediated alleviating of hepatic fibrosis.

### *MBL Prompts Senescence of HSCs Through Mammalian Target of Rapamycin/p53/p21 Signaling Pathway*

Our pilot immunofluorescence assay showed that MBL is colocalized with  $\alpha$ -SMA in fibrotic liver sections in mice (Figure 8A) or human beings (Figure 8B), where p53 expression was notably higher in MBL<sup>+</sup> $\alpha$ -SMA<sup>+</sup> activated HSCs than in MBL<sup>-</sup> $\alpha$ -SMA<sup>+</sup> cells (Figure 8B). Together with our previous study showing that MBL could interact with HSCs in which MBL was hardly detected,<sup>15</sup> these results prompt us to explore whether MBL could affect the senescence of HSCs. Here, we treated human HSC line LX-2 with or without the senescence inducer H<sub>2</sub>O<sub>2</sub>,<sup>27</sup> which could trigger the cellular senescence of HSCs, along with MBL protein or not. As anticipated, H<sub>2</sub>O<sub>2</sub> did induce the senescence of LX-2 cells, indicated by more SA- $\beta$ -Gal expression (Figure 9A), more robust cellular growth arrest (Figure 9B), and increased protein expression and mRNA level of senescence-related molecules (Figure 9C and D). However, MBL treatment could significantly promote H<sub>2</sub>O<sub>2</sub>-induced cellular senescence (Figure 9), and synergistically reduce the mRNA level of fibrosis-associated genes with H<sub>2</sub>O<sub>2</sub>-treatment (Figure 9E). Although MBL treatment alone does not affect the senescence (Figure 9) or viability of LX-2 cells (Figure 9F), these results indicated that MBL promoted HSC senescence.

A previous study showed that p53 is a vital molecule involved in HSC senescence,<sup>28</sup> in which mammalian target of rapamycin (mTOR)/p53/p21 is considered one of the classic senescent pathways.<sup>29</sup> Our pilot Western blot analysis showed that phosphatidylinositol-3-kinase (PI3K)/AKT/mTOR signaling was up-regulated in the liver tissues

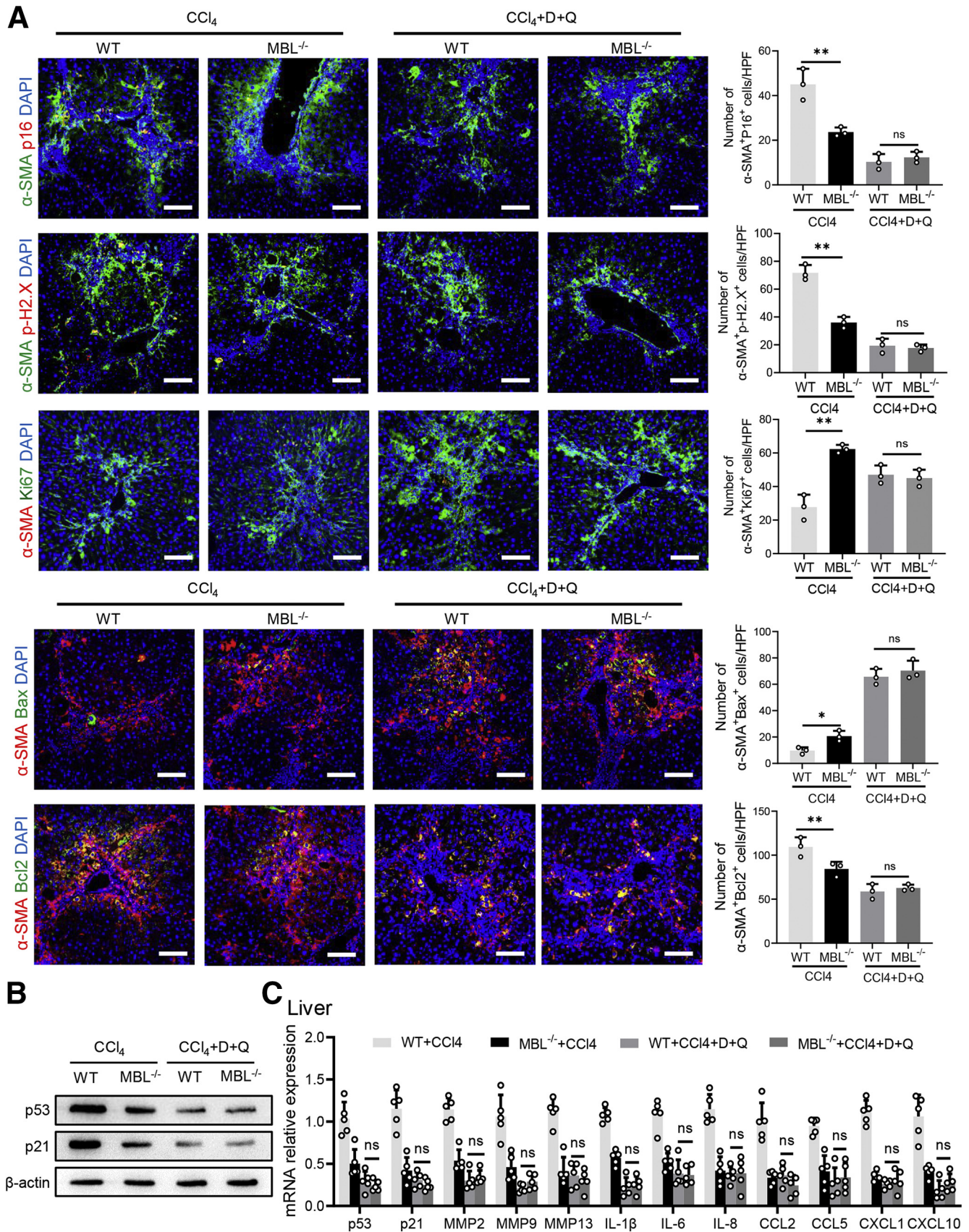
of WT mice compared with MBL<sup>-/-</sup> mice during pAAV-control administration, which was abrogated by pAAV-MBL treatment (Figure 10A). Furthermore, we observed that intraperitoneal injection of rapamycin did inhibit mTOR/p53/p21 activation in vivo during fibrosis establishment (Figure 10B and C). This rapamycin administration eliminated MBL deficiency-mediated differences in hepatic fibrosis degree and HSC senescence (Figure 10C-E). Together with the earlier results about p53 and p21, we proposed that the mTOR/p53/p21 pathway might be involved in MBL-mediated HSC senescence. Similar to these results, MBL treatment substantially promoted senescence of LX-2 cells, indicated by increased frequency of SA- $\beta$ -GAL<sup>+</sup> cells, stronger cellular growth arrest, increased protein expression (p53 and p21), and mRNA levels of senescence-related molecules, as well as the reduced mRNA levels of fibrosis-associated genes (Figure 11). However, this MBL-induced senescence-promoting effect was abolished by pretreatment with the p53-specific inhibitor pifithrin- $\alpha$  (PFT- $\alpha$ ) (Figure 11), or the mTOR-suppressor rapamycin (Figure 12), ahead of the exposure to MBL and H<sub>2</sub>O<sub>2</sub>, as shown by the comparable frequency of SA- $\beta$ -GAL<sup>+</sup> cells, cellular growth arrest, protein expression, and mRNA levels of senescence-related molecules in MBL-treated or untreated cells. Together, these results implied that MBL promoted senescence of HSCs via the mTOR/p53/p21 pathway.

### *MBL Promotes HSC Senescence Through Interaction With Cell Surface Calreticulin*

According to our previous study, MBL could bind to the T-cell surface with calreticulin (CRT) and subsequently activate the downstream pathway.<sup>30</sup> CRT, which is expressed in various cell types, including HSCs,<sup>31</sup> can signal in association with low-density lipoprotein receptor-related protein 1 (LRP1), thus leading to the activation of the PI3K/AKT/mTOR pathway.<sup>32,33</sup> Our pilot experiment showed that MBL is bound to cell-surface CRT in the human HSC line LX-2 (Figure 13A). In addition, when we incubated primary mouse HSCs with the supernatant harvested from stimulated primary mouse hepatocytes, the fluorescence staining showed the colocalization of MBL and CRT on the cell surface of HSCs, accompanied by the up-regulated activation of the mTOR/p53/p21 signaling pathway (Figure 13B-E). To define whether MBL binding to CRT subsequently can regulate the downstream mTOR activation and further affect the senescence of HSCs, we used CRT blocking antibody to inhibit the potential binding of CRT and MBL.<sup>30</sup> The results showed that the anti-CRT pretreatment completely blocked the MBL-mediated promotion of senescence, as indicated by comparable SA- $\beta$ -GAL positivity (Figure 14A), cellular growth arrest (Figure 14B), and mRNA levels of senescence-related genes (Figure 14C) in cells treated with MBL or not. Interestingly, we observed that MBL increased the cell-surface CRT-LRP1 interaction while not affecting their surface expression (Figure 14D). As illustrated in Figure 14E, LX-2 cells exposed to MBL and H<sub>2</sub>O<sub>2</sub> showed an increased intracellular level of catalytic subunit p110 of

PI3K and its interaction with LRP1, and the association of LRP1 and Rab8. Moreover, MBL drastically increased p110 level and Akt phosphorylation, as well as activation of

the mTOR/p53/p21 pathway as determined by immunoblotting, which was notably inhibited by anti-CRT pretreatment (Figure 14F). Anti-CRT treatment also abolished



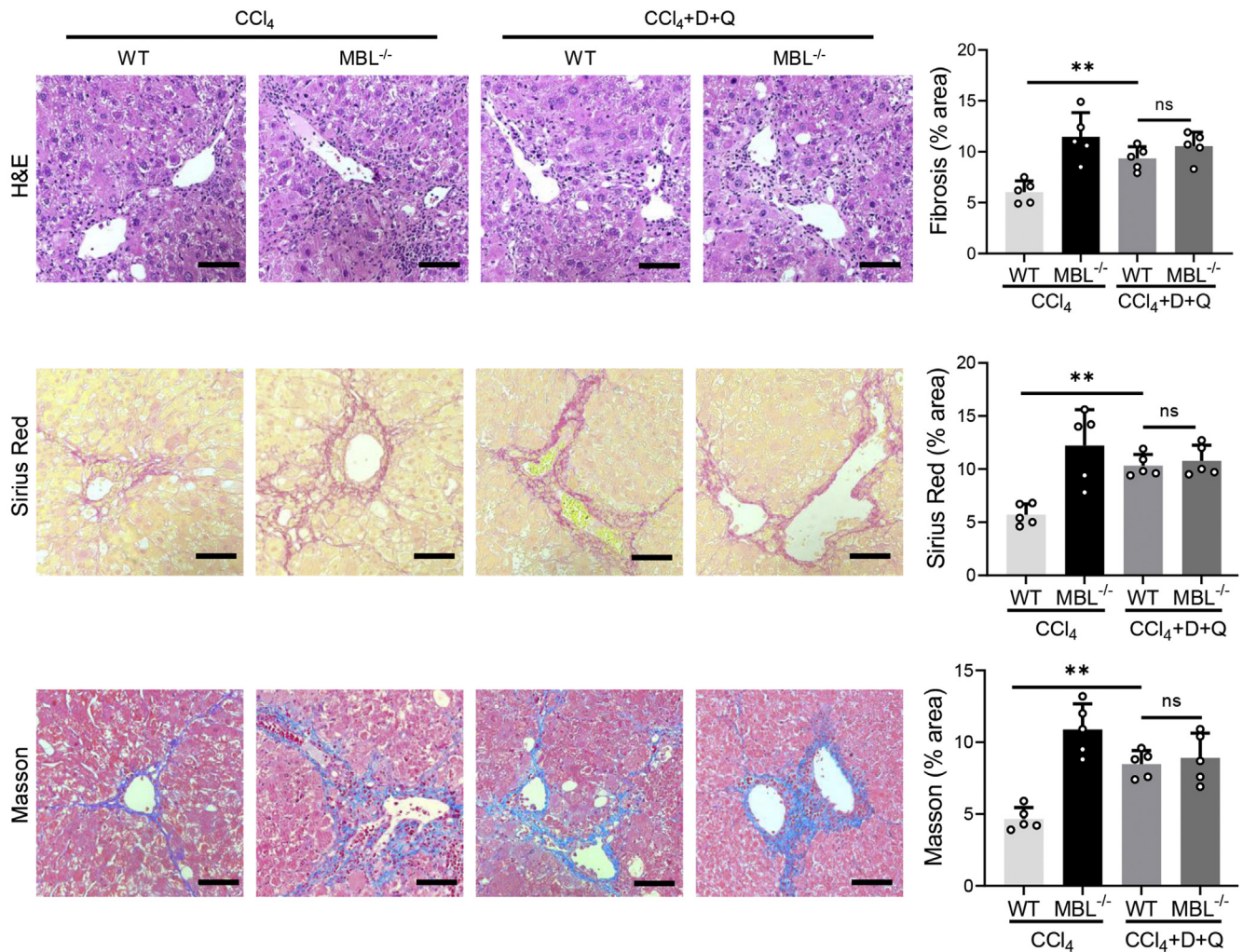


**Figure 7. Senolytic treatment inhibits MBL-mediated amelioration of liver fibrosis.** The MBL<sup>-/-</sup> and WT mice (n = 6 per group) were garaged with D+Q every 3 weeks for 3 times during the fibrosis establishment. Representative photomicrographs of H&E staining, Sirius Red, and Masson's trichrome staining in liver sections. Scale bars: 100  $\mu$ m. Data are presented as means  $\pm$  SEM. \*\**P* < .01, 1-way analysis of variance followed by Tukey post hoc tests for multiple group comparisons.

the MBL-mediated reduced mRNA levels of fibrosis-associated genes in LX-2 cells upon MBL treatment (Figure 14G). These results suggest that MBL binds to the membrane CRT of HSCs, promoting HSC senescence.

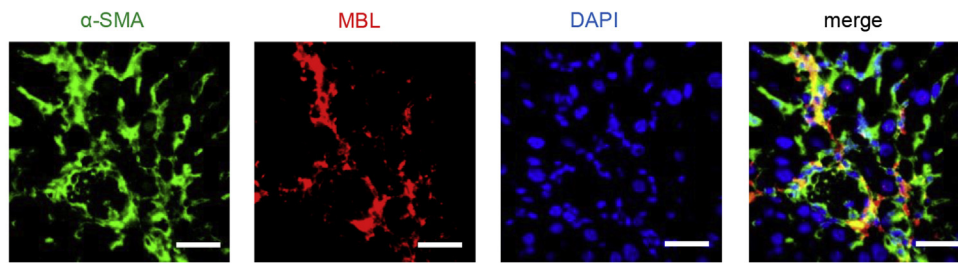
## Discussion

In this study, we have made novel findings toward a better understanding of MBL function in the liver micro-environment. We first discovered that MBL levels increase

markedly in the liver upon hepatic fibrogenesis, whereas they decrease when fibrosis progresses. Genetic deficiency of MBL exacerbates liver fibrotic pathologies mediated by the reduction of HSC senescence, which is abolished by hepatic MBL restoration. One of the underlying mechanisms is that MBL directly interacts with cell-surface CRT, which further signals in association with LRP1, leading to PI3K/Akt activation and downstream mTOR/p53/p21 pathway, thus promoting cellular senescence of HSCs and relieving liver fibrosis progression. Hence, MBL expression and its

**Figure 6. (See previous page). Senolytic treatment eliminates senescent cells in mice fibrotic livers.** The MBL<sup>-/-</sup> and WT mice (n = 6 per group) were garaged with D+Q every 3 weeks for 3 times during the fibrosis establishment. (A) Representative immunofluorescence staining of  $\alpha$ -SMA (green) and p16 (red), p-H2.X (red), or Ki67 (red) in liver tissues. (B) Representative immunofluorescence staining of  $\alpha$ -SMA (red) and Bax (green) or Bcl2 (green) in liver tissues. (C) The p53 and p21 protein levels in liver tissues were assessed by Western blot analysis. (D) The mRNA levels of senescence-related genes in liver tissues were assessed by quantitative reverse-transcription PCR analysis. Scale bars: 100  $\mu$ m. Data are presented as means  $\pm$  SEM. \**P* < .05, \*\**P* < .01, 1-way analysis of variance followed by Tukey post hoc tests for multiple group comparisons. CCL, chemokine (C-C motif) ligand; CXCL, chemokine (C-X-C motif) ligand; DAPI, 4',6-diamidino-2-phenylindole; HPF, high-power field; IL, interleukin; MMP, matrix metalloproteinase.

## A Mice



## B Human

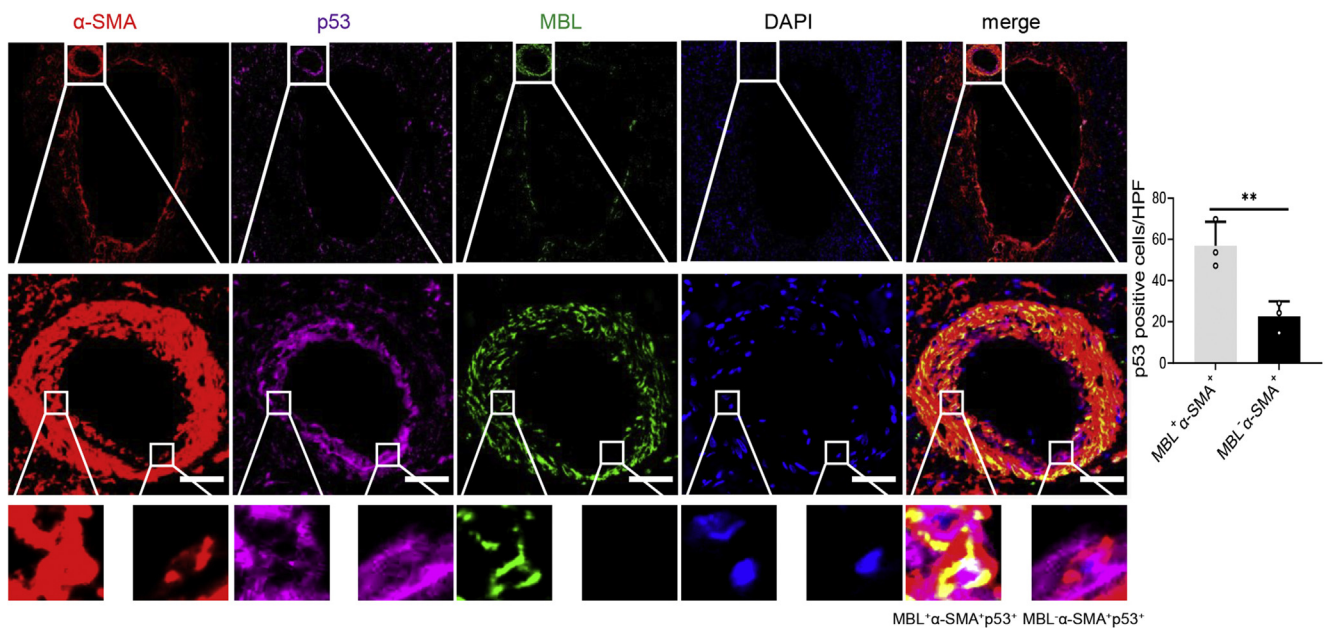


**Figure 8. MBL co-localizes with senescent HSCs in vivo.** (A) Representative photomicrographs of colocalization of MBL (red) and  $\alpha$ -SMA (green) in liver tissues of WT mice by immunofluorescence analysis. Scale bars: 50  $\mu$ m. (B) Representative photomicrographs of colocalization of  $\alpha$ -SMA (red), MBL (green), and p53 (purple) expression in liver tissues of cirrhotic patients by immunofluorescence analysis. Scale bars: 25  $\mu$ m. Data are presented as means  $\pm$  SEM. \*\* $P < .01$ , Student  $t$  test. DAPI, 4',6-diamidino-2-phenylindole; HPF, high-power field.

association with HSCs control hepatic fibrosis by promoting HSC senescence, implying that MBL might serve as a bona fide regulator of liver fibrosis progression and potential targets for antihepatic fibrosis therapies.

MBL, as a primarily liver-derived soluble opsonin, holding a critical position in innate immunity mainly through initiating lectin pathway activation, also can serve multiple modulatory functions apart from complement activation in tissue homeostasis and various diseases.<sup>10,16,17,34</sup> In addition, MBL has been described as an acute-phase protein that increases and plays vital roles in the acute-phase response.<sup>35,36</sup> Local inflammation or injuries in the liver during hepatic fibrosis could induce the acute-phase protein expression to maintain homeostasis and tissue repair.<sup>37,38</sup> Therefore, it is not surprising that our current study found that plasma MBL levels were higher in cirrhosis patients than in healthy controls.

However, we observed that plasma MBL levels and MBL expression in liver tissues were correlated inversely with cirrhosis severity. These results were partially supported by a previous study indicating lower MBL levels in patients with more advanced stages of cirrhosis.<sup>18</sup> An early study also showed that coding mutation homozygosity O/O associated with lower MBL expression was related to advanced liver fibrosis in hepatitis C virus patients.<sup>19</sup> This evidence suggests that the polymorphism of the MBL gene in patients with different stages of cirrhosis results in the differences of maximal MBL expression among these patients. Furthermore, because our current work suggests that hepatic MBL contributes to the amelioration of fibrosis progression, patients with lower MBL expression thus have less MBL-mediated control of fibrosis deterioration and might suffer from severer liver cirrhosis. Because our findings suggest that MBL has a potential role in liver

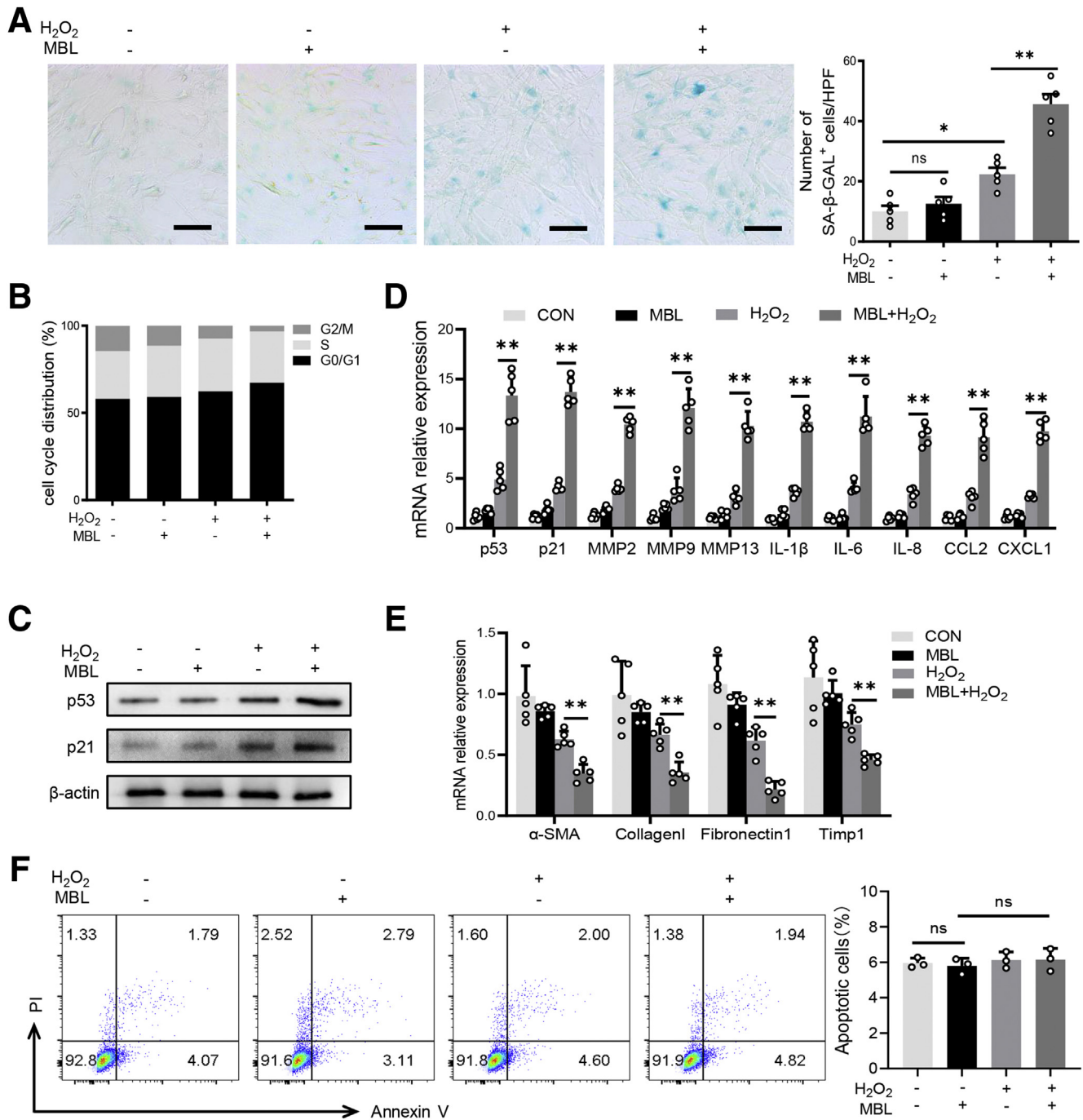


**Figure 9. MBL prompts senescence of HSCs in vitro.** LX-2 cells were treated with MBL (10  $\mu$ g/mL) and/or H<sub>2</sub>O<sub>2</sub> (300  $\mu$ mol/L) for 48 hours. (A) Representative images of the SA- $\beta$ -gal staining of LX-2 cells treated with or without MBL and/or H<sub>2</sub>O<sub>2</sub>. (B) The distribution of cell cycle on the treated LX-2 cells with flow cytometry analysis. (C) The p53 and p21 protein levels were assessed by Western blot analysis. (D) The mRNA levels of senescence-related genes were assessed by quantitative reverse-transcription (qRT)-PCR analysis. (E) The mRNA levels of fibrosis-associated genes were assessed by qRT-PCR analysis. (F) The apoptosis on the treated LX-2 cells with flow cytometry analysis. Scale bars: 100  $\mu$ m. Data are presented as means  $\pm$  SEM. \* $P$  < .05, \*\* $P$  < .01, 1-way analysis of variance followed by Tukey post hoc tests for multiple group comparisons. The data shown represent 3 independent experiments. CON, control; CXCL, chemokine (C-X-C motif) ligand; HPF, high-power field; IL, interleukin; MMP, matrix metalloproteinase; TIMP1, tissue inhibitors of metalloproteinase 1.

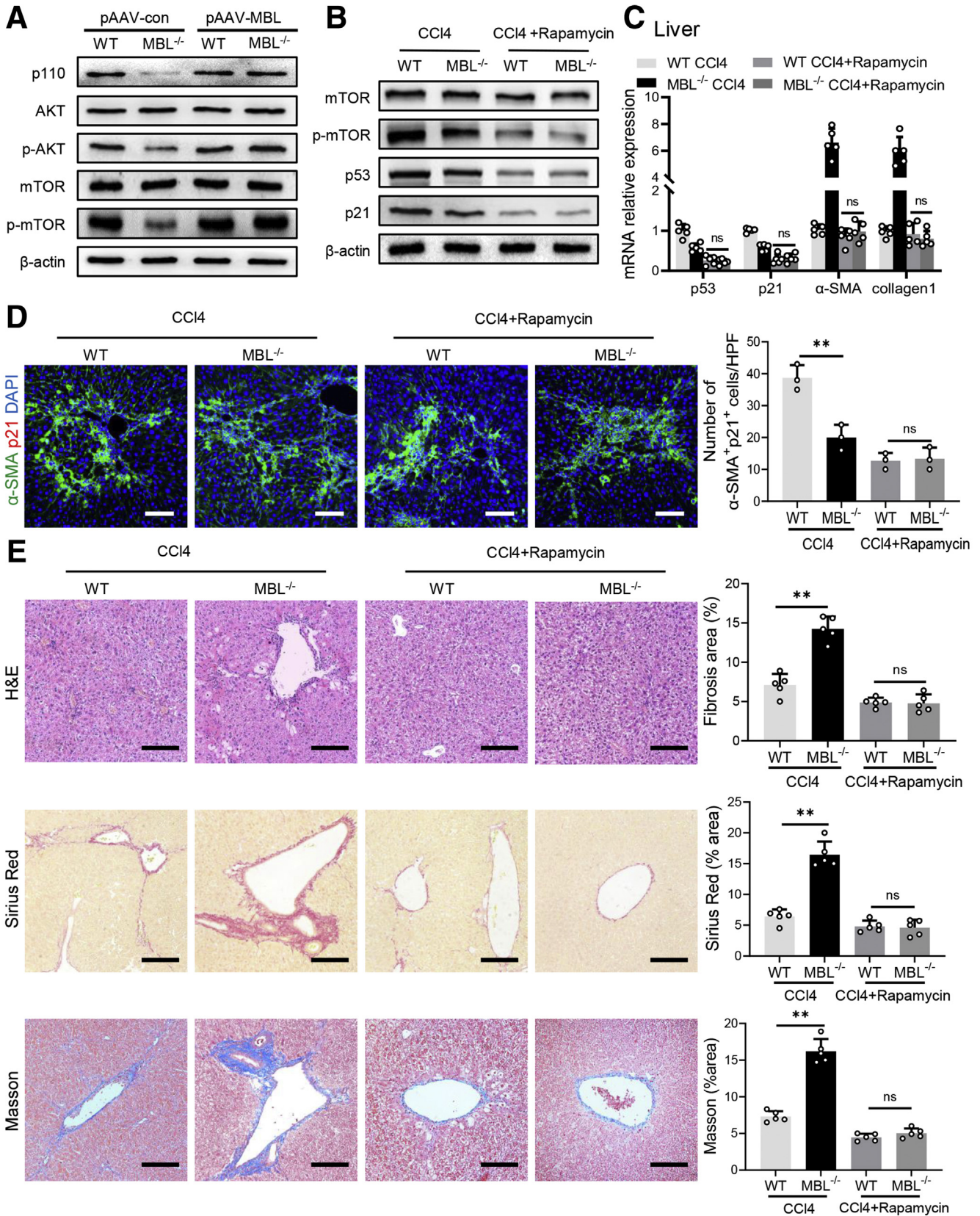
fibrosis, we decided to address its exact positions. While using MBL-deficient mice, we discovered that genetic depletion of MBL did lead to a notable deterioration of

hepatic fibrosis. Given that the liver, particularly hepatocytes, is a key source of MBL,<sup>11,12,39-41</sup> our recent studies have established liver-specific AAV vectors carrying the

MBL gene that could restore hepatic MBL expression.<sup>13,15</sup> Accordingly, in the current study, restoration of hepatic MBL expression with pAAV-MBL nearly completely abrogated the liver fibrosis aggravation owing to MBL absence,

providing evidence that MBL contributes to the amelioration of hepatic fibrosis.

Located in the liver microenvironment, activated HSCs represent the dominant profibrogenic cell population,



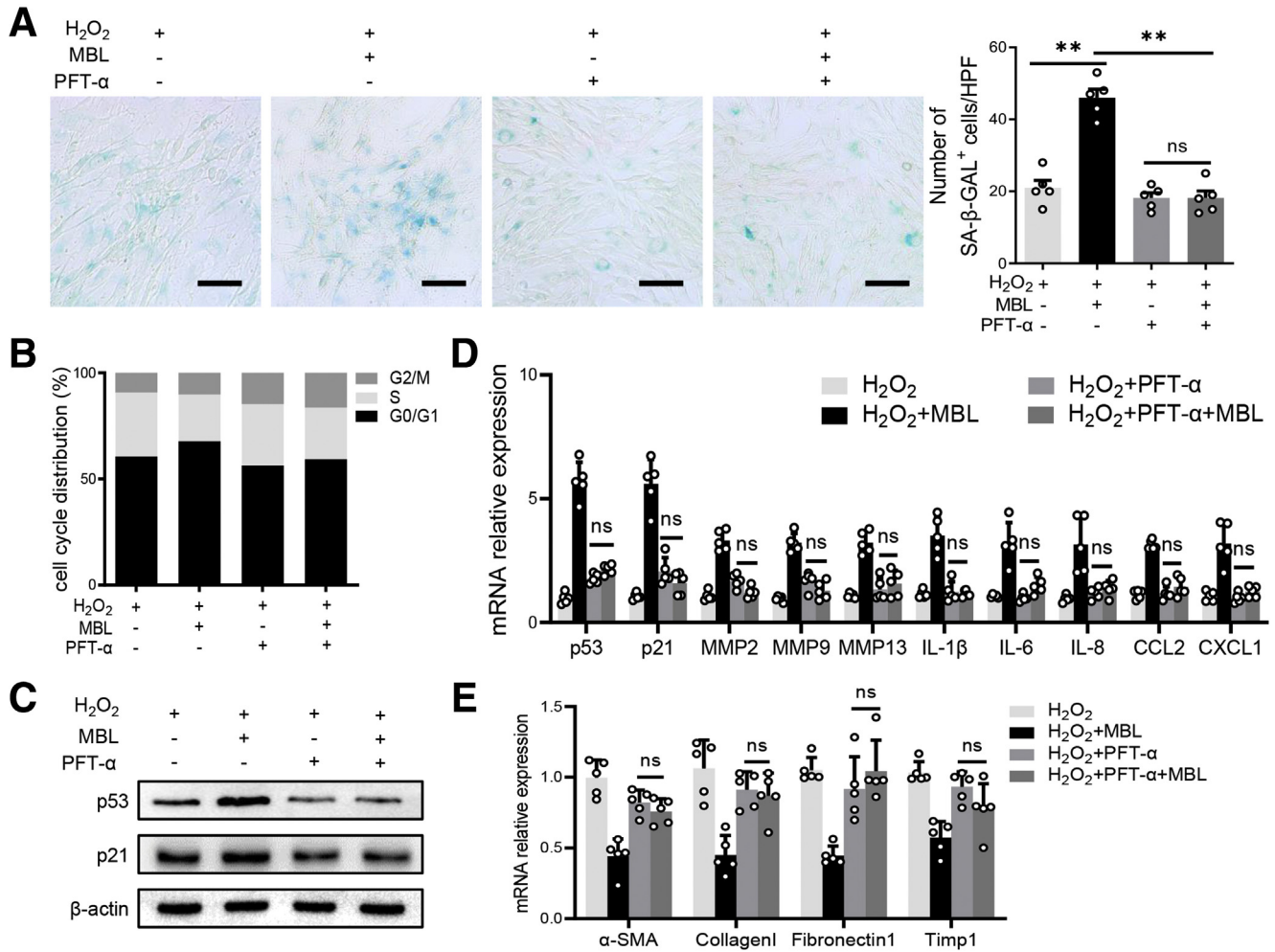


**Figure 11. MBL prompts HSC senescence via the p53/p21 pathway.** LX-2 cells were treated with PFT-α (10 μmol/L) 2 hours before the incubation of MBL and H<sub>2</sub>O<sub>2</sub>. (A) Representative photomicrographs of the SA-β-gal staining of LX-2 cells treated with PFT before the incubation of MBL. (B) The distribution of cell cycle on the treated LX-2 cells with flow cytometry analysis. (C) The p53 and p21 protein levels were assessed by Western blot analysis. (D) The mRNA levels of senescence-related genes were assessed by quantitative reverse-transcription (qRT)-PCR analysis. (E) The mRNA levels of fibrosis-associated genes were assessed by qRT-PCR analysis. Scale bars: 100 μm. Data are presented as means ± SEM. \*\**P* < .01, 1-way analysis of variance followed by Tukey post hoc tests for multiple group comparisons. The data shown represent 3 independent experiments. CXCL, chemokine (C-X-C motif) ligand; HPF, high-power field; IL, interleukin; MMP, matrix metalloproteinase; TIMP1, tissue inhibitors of metalloproteinase 1.

contributing to most ECM-producing myofibroblasts responsible for liver fibrogenesis.<sup>42-44</sup> Although still controversial, emerging evidence suggests that the senescence of activated HSCs improves hepatic fibrosis by eliminating the major source of ECM.<sup>20,23,24,45</sup> Furthermore,

cellular senescence, as a sustained state of cell-cycle arrest, could promote tissue remodeling after injury and play crucial roles in CLD.<sup>46</sup> Therefore, we propose that activated HSC senescence might be associated with MBL-mediated amelioration of hepatic fibrosis progression. Indeed, we

**Figure 10. (See previous page). Rapamycin treatment abrogates MBL-mediated amelioration of liver fibrosis.** WT and MBL<sup>-/-</sup> mice (n = 5 per group) were treated with pAAV-control or pAAV-MBL vectors before the establishment of liver fibrosis. (A) The protein levels of p110, mTOR, p-mTOR, AKT, and p-AKT in liver tissues were assessed by Western blot analysis. The MBL<sup>-/-</sup> and WT mice (n = 5 per group) were injected intraperitoneally with rapamycin (1 mg/kg body weight/d) during the fibrosis establishment. (B) The protein levels of mTOR, p-mTOR, p53, and p21 in mouse liver were assessed by Western blot analysis. (C) The mRNA levels of p53, p21, α-SMA, and collagen 1 were assessed by quantitative reverse-transcription PCR. (D) Representative immunofluorescence staining of α-SMA (green) and p21 (red) in liver sections. (E) Representative photomicrographs of H&E, Sirius Red, and Masson's trichrome staining in the liver tissues. Scale bars: 100 μm. Data are presented as means ± SEM. \*\**P* < .01, 1-way analysis of variance followed by Tukey post hoc tests for multiple group comparisons. DAPI, 4',6-diamidino-2-phenylindole; HPF, high-power field.

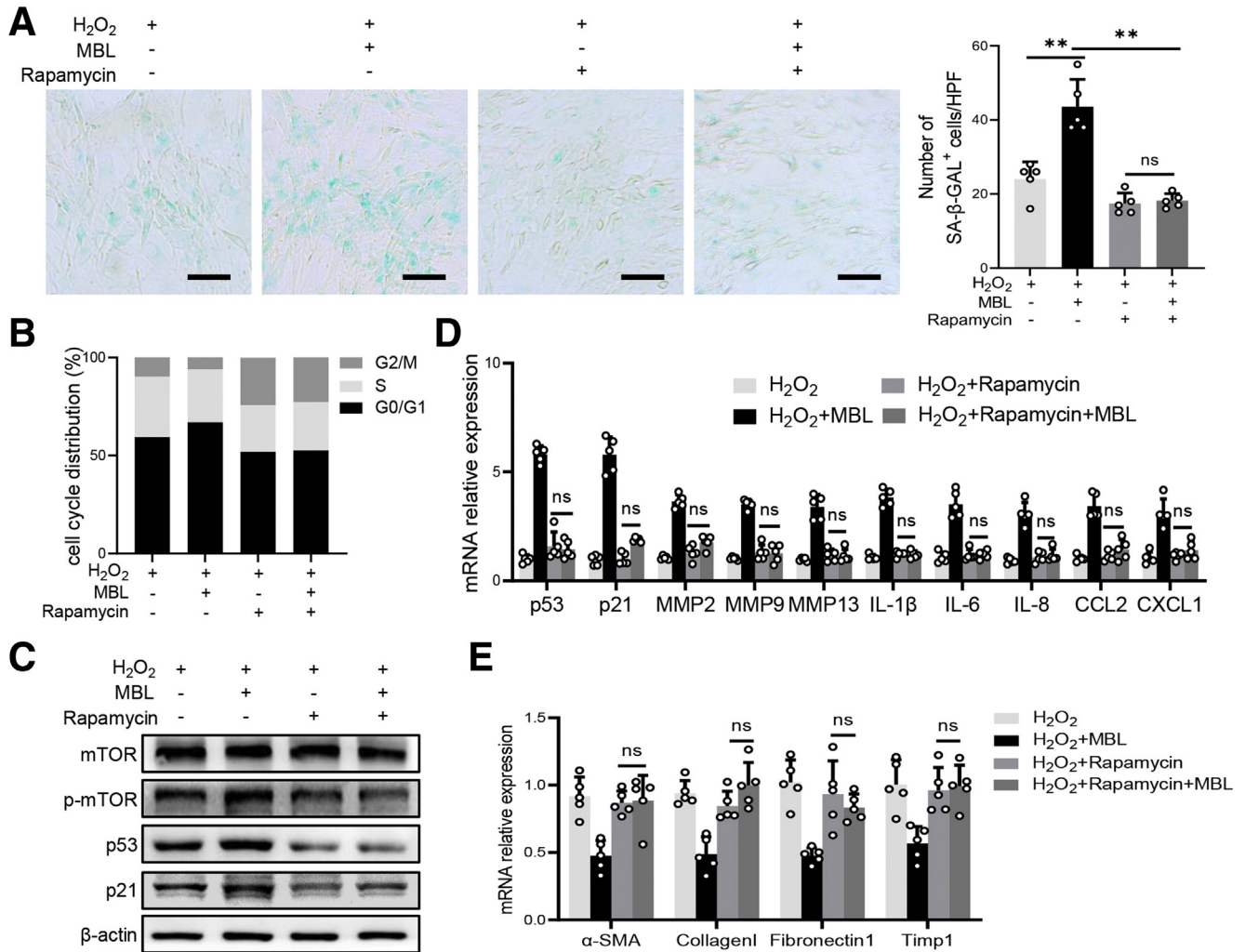


**Figure 12. The mTOR/p53/p21 pathway is involved in the MBL-mediated promotion of HSC senescence.** LX-2 cells were treated with rapamycin (100 nmol/L) 2 hours before the incubation of MBL and H<sub>2</sub>O<sub>2</sub>. (A) Representative photomicrographs of the SA-β-gal staining of LX-2 cells treated with rapamycin before the incubation of MBL. (B) The distribution of cell cycle on the treated LX-2 cells with flow cytometry analysis. (C) The p53, p21, mTOR, and p-mTOR protein levels were assessed by Western blot analysis. (D) The mRNA levels of senescence-related genes were assessed by quantitative reverse-transcription (qRT)-PCR analysis. (E) The mRNA levels of fibrosis-associated genes were assessed by qRT-PCR analysis. Scale bars: 100 μm. Data are presented as means ± SEM. \*\**P* < .01, 1-way analysis of variance followed by Tukey post hoc tests for multiple group comparisons. The data shown represent 3 independent experiments. CCL, chemokine (C-C motif) ligand; CXCL, chemokine (C-X-C motif) ligand; HPF, high-power field; IL, interleukin; MMP, matrix metalloproteinase.

showed that the frequency of senescent activated HSCs markedly decreased in MBL-deficient mice compared with those in WT controls. In addition, the subsequent restoration of hepatic MBL expression with pAAV-MBL could eliminate the reduction of senescent HSCs in MBL-deficient mice. Although there have not been any drugs to eliminate only senescent HSCs selectively, senolytic drugs such as D+Q, a prominent senotherapeutic strategy,<sup>47</sup> can efficiently deplete senescent HSCs in the liver.<sup>26</sup> In the current study, we found that senolytic drugs (D+Q) dramatically reduced senescent activated HSCs in the liver. Most importantly, these senolytic drugs could eliminate the differences of liver fibrosis features between WT and MBL<sup>-/-</sup> mice. Apparently, our current work suggests that HSC senescence is involved in MBL-mediated alleviation of hepatic fibrosis

progression, although senescence of other cells could not be excluded. Of note, senolytics D+Q could exacerbate hepatic fibrosis in WT mice with MBL expression. This result is different from a previous report indicating that the senolytic fisetin reduced cholangiocyte senescence and improved fibrosis in the *Mdr2*<sup>-/-</sup> mouse.<sup>48</sup> One possible reason for the different findings and outcomes between these 2 studies is that the murine fibrosis models' mechanisms differ significantly. The *Mdr2*<sup>-/-</sup> mouse model spontaneously develops primary sclerosing cholangitis and progressive secondary biliary fibrosis owing to accumulation of toxic bile acids in hepatocytes and initiation of a profibrogenic cholangiocyte response.<sup>49</sup> Emerging evidence has indicated that CCL<sub>4</sub> metabolized in the liver induces hepatocyte apoptosis, leading to parenchymal liver damage and HSC activation,



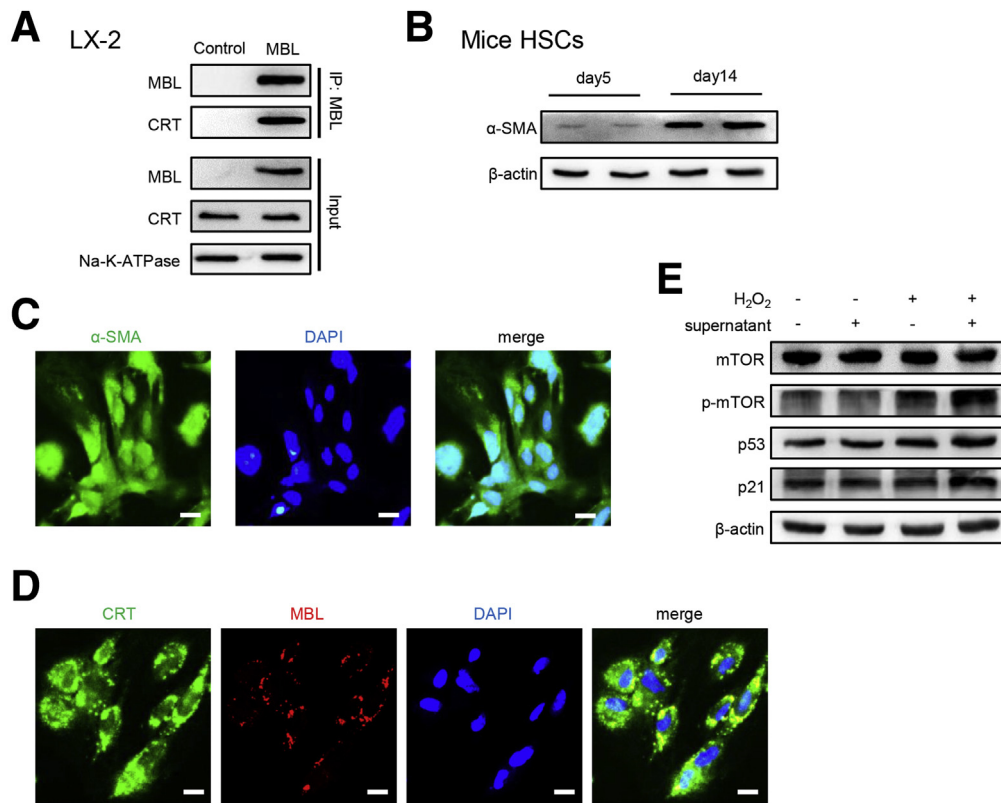


**Figure 13. MBL binds to CRT on the cell surface of HSCs.** (A) LX-2 cells were incubated with MBL protein and the membrane fractions were extracted for subsequent immunoprecipitation. The association of MBL with CRT was determined by immunoblotting of immunoprecipitates with anti-CRT. (B) HSCs were extracted from the mouse liver and cultured for 14 days, followed by incubation with primary hepatocyte supernatants. The protein levels of  $\alpha$ -SMA of HSCs on day 5 and day 14. (C) Representative immunofluorescence staining of  $\alpha$ -SMA (green) in HSCs on day 14. (D) Representative immunofluorescence staining of  $\alpha$ -SMA (green) and MBL (red) in HSCs stimulated with primary hepatocytes supernatants. (E) The protein levels of mTOR, p-mTOR, p53, and p21 in HSCs stimulated with primary hepatocyte supernatants. Scale bars: 25  $\mu$ m. The data shown represent 3 independent experiments. ATPase, adenosine triphosphatase; DAPI, 4',6-diamidino-2-phenylindole.

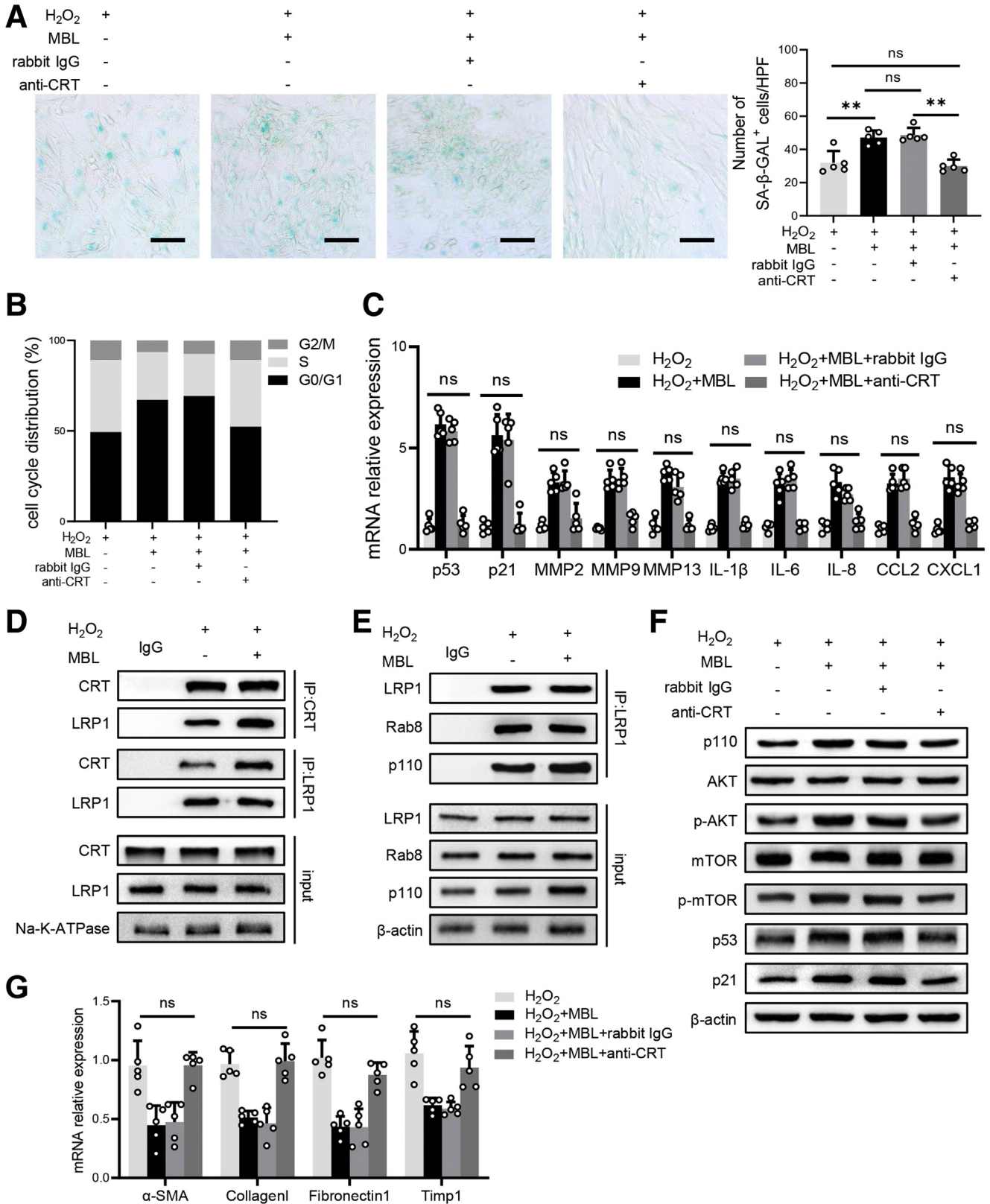
favoring the fibrogenic process.<sup>50</sup> Notably, CCl<sub>4</sub>-induced hepatic fibrosis starts from the hepatic centrilobular zone 3 and progresses toward the portal tracts of zone 1, opposite the biliary fibrosis in Mdr2<sup>-/-</sup> mice.<sup>51</sup> Another reason might be that the distinct senolytics are likely to target different cells and work differently at various time points in these 2 models. Although all senolytic drugs appear to clear senescent cells, each drug's exact roles and mechanisms, especially in different contexts in vivo, still are unclear.<sup>52,53</sup> Even though it has been reported that D+Q showed selective cytotoxicity toward senescent HSCs,<sup>26</sup> the study mentioned earlier indicated that fisetin selectively eliminated senescent cholangiocytes, whereas D+Q targeted both proliferating and senescent cholangiocytes.<sup>48</sup> Furthermore, we performed senolytic administration ahead of CCl<sub>4</sub> injection to ensure the depletion of senescent HSCs in the present study, whereas the report mentioned earlier only focused on the senescent cholangiocytes.<sup>48</sup> Therefore, although the exact mechanisms need to be explored further and other senescent cells involved could not be excluded, it is not surprising that the difference in findings of the roles of these distinct senolytics in our present study and the report mentioned above.<sup>48</sup>

The fate of activated HSCs is orchestrated by an interdependent network of molecular and cellular components in the liver microenvironment.<sup>8,9,54</sup> However, the underlying mechanisms of HSC senescence induction still are unclear. In this study, we observed MBL<sup>+</sup> $\alpha$ -SMA<sup>+</sup> activated HSCs in the liver fibrotic sections, in which the senescent marker p53 was expressed. This finding was partially supported by our previous study showing the colocalization of MBL and  $\alpha$ -SMA<sup>+</sup> activated HSCs in the peritumor region in HCC.<sup>15</sup> Together with our earlier finding that MBL was hardly detected in HSCs but could interact directly with HSCs,<sup>15</sup> these data prompt us to investigate the underlying mechanisms of the interaction between MBL protein and HSCs and the downstream signaling pathway. Intriguingly, while using H<sub>2</sub>O<sub>2</sub> to induce HSC senescence, MBL treatment markedly promoted the senescence of HSCs. Meanwhile, mTOR/p53/p21, as a classic senescent pathway,<sup>21,55</sup> was up-regulated by MBL. Nevertheless, this regulatory role was eliminated by selective inhibitors of mTOR or p53, indicating their involvement in MBL-mediated HSC senescence.

Given our previous reports showing that MBL binds to CRT on the T-cell surface,<sup>30</sup> as well as the presence of CRT on the cell surface of LX-2 cells<sup>56</sup> and activated HSCs,<sup>31</sup> we

subsequently blocked the CRT-MBL interaction with anti-CRT. As expected, anti-CRT pretreatment completely blocked the MBL-mediated pro-growth senescence, MBL-up-regulated PI3K/Akt pathway, and downstream

mTOR/p53/p21 signaling in LX-2 cells. Furthermore, coculture of primary mouse HSCs with hepatocyte supernatant also resulted in CRT-MBL colocalization and mTOR/p53/p21 signaling pathway activation in HSCs, suggesting



hepatocyte-secreted MBL could interact with CRT and up-regulate the mTOR/p53/p21 signaling pathway. Intriguingly, MBL treatment strengthened the interaction of LRP1 and CRT on the cell surface, which might be explained by previous studies showing the cell surface CRT-MBL interaction<sup>31</sup> and the MBL binding to cell surface LRP1 (CD91).<sup>57</sup> Of note, we discovered that MBL interaction with CRT increased the intracellular level of catalytic subunit p110 of PI3K bound to LRP1 associated with Rab8. These results were supported by a previous report indicating that the Toll-like receptors, which are pattern recognition receptors such as MBL, could crosstalk and activate LRP1, which recruits a Rab8a/PI3K complex, and that further activates Akt/mTOR signaling.<sup>33</sup> In addition, the present results could be explained by the previous observation that cell surface CRT signals in association with LRP1 by forming a CRT-LRP1-receptor complex. Furthermore, it is reported that tissue-type-plasminogen activator, as a ligand of LRP1, mediated the resolution of CCl<sub>4</sub>-induced acute liver injury through triggering LRP1-associated signaling in HSCs, which might lead to the regression of activated HSCs in vivo.<sup>58</sup> Thus, our present findings provide new insights into the mechanisms underlying MBL-mediated HSC senescence upon stress.

In summary, our data provide compelling evidence that MBL is essential for controlling liver fibrosis progression, broadening the knowledge of MBL biologic function. In addition, this effect is partially mediated through MBL binding to the cell surface CRT of HSCs, facilitating CRT-LRP1 interaction and further activating the downstream mTOR/p53/p21 signaling pathway that promotes cellular senescence. These findings elucidate a previously unrecognized senescence-promoting role of MBL in the liver microenvironment that contributes to the control of hepatic fibrosis progression and provides a whole new perspective for antifibrotic therapy based on MBL expression.

## Materials and Methods

### Reagents and Antibodies

Rapamycin, a selective mTOR inhibitor, was purchased from MCE company (Monmouth Junction, NJ). PFT- $\alpha$ , a selective inhibitor of p53, was obtained from Selleck Chemicals (Houston, TX). The MBL protein was extracted and purified as we described previously.<sup>30</sup> H<sub>2</sub>O<sub>2</sub> and CCl<sub>4</sub> were purchased from Sigma Technology (Waltham, MA). A prestained protein ladder (26616, 26625) was bought from

ThermoFisher Scientific Company. Rabbit anti- $\alpha$ -SMA antibody (ab5694), mouse anti- $\alpha$ -SMA antibody (ab7817), human MBL antibody (ab23457), CRT antibody (ab2907, ab22683), horseradish peroxidase (HRP)-conjugated goat anti-rabbit IgG (ab6721), HRP-conjugated goat anti-mouse IgG (ab6789), fluorescein isothiocyanate-conjugated goat anti-rabbit IgG (ab6717), fluorescein isothiocyanate-conjugated goat anti-mouse IgG (ab6785), Cy3-conjugated goat anti-mouse IgG (ab97035), Cy3-conjugated goat anti-rabbit IgG (ab6939) were all from Abcam (Cambridge, UK). Rabbit anti-Ki67 antibody (clone D3B5), AKT antibody (4691S), phospho-AKT antibody (4060S), mTOR antibody (983S), phospho-mTOR antibody (5536S), Na/K-adenosine triphosphatase (3010S), LRP1 (64099S), and phospho-histone H2A.X antibody (9718S) were all obtained from Cell Signaling Technology (Danvers, MA). Mouse anti-mouse MBL-C antibody (clone 14D12, NBP1-60128) was purchased from R&D Systems (Minneapolis, MN). PI3K antibody (21739-1-AP), Rab8 antibody (55296-1-AP), p53 antibody (60283-2-Ig), p21 antibody (10355-1-AP), p16 antibody (10883-1-AP), Bax antibody (50599-2-Ig), and Bcl2 antibody (12789-1-AP) were supplied by Proteintech (Chicago, IL). Lipopolysaccharide was from MCE Company.

### Animals

All animal experiments in this study were performed in accordance with the guidance of the Welfare and Ethical Committee for Experimental Animal Care of Southern Medical University. WT C57BL/6J mice were purchased from the Animal Center of Southern Medical University (Guangzhou, China). MBL<sup>-/-</sup> mice on a C57BL/6J background were purchased from the Jackson Laboratory (Bar Harbor, ME). The animals were housed under a 12-hour light/dark cycle in a specific pathogen-free animal condition with a controlled temperature (20°C–25°C) and humidity (50%  $\pm$  5%). Female 6- to 8-week-old mice were used for all experiments.

### Model of Liver Fibrosis

Mouse models of liver fibrosis were established according to the previously reported method with minor modification.<sup>59</sup> Mice were injected intraperitoneally with 25% CCl<sub>4</sub> (Macklin, Shanghai, China) at a dose of 1  $\mu$ L/g 3 times a week for 6 weeks, and were killed 2 days after the last injection of CCl<sub>4</sub> for further analysis. To eliminate the

**Figure 14.** (See previous page). **MBL-CRT interaction up-regulates the association of CRT and LRP1 and downstream senescent-related signaling pathways in HSC.** LX-2 cells were treated with CRT antibody or IgG 1 hour before the incubation of MBL and H<sub>2</sub>O<sub>2</sub>. (A) Representative photomicrographs of the SA- $\beta$ -gal staining of LX-2 cells. (B) The distribution of cell cycle on the treated LX-2 cells with flow cytometry analysis. (C) The mRNA levels of senescence-related genes were assessed by quantitative reverse-transcription (qRT)-PCR analysis. (D) The association of CRT and LRP1 was determined by immunoblotting of immunoprecipitates in membrane fractions of LX-2 cells. (E) The association of LRP1, Rab8, and p110 was determined by immunoblotting of immunoprecipitates in cytoplasm fractions of LX-2 cells. (F) The p53, p21, mTOR, p-mTOR, AKT, p-AKT, and p110 protein levels were assessed by Western blot analysis. (G) The mRNA levels of fibrosis-associated genes were assessed by qRT-PCR analysis. *Scale bars:* 100  $\mu$ m. Data are presented as means  $\pm$  SEM. \*\**P* < .01, Student *t* test or 1-way analysis of variance followed by Tukey post hoc tests for multiple group comparisons. The data shown represent 3 independent experiments. ATPase, adenosine triphosphatase; CCL, chemokine (C-C motif) ligand; CXCL, chemokine (C-X-C motif) ligand; HPF, high-power field; IL, interleukin; MMP, matrix metalloproteinase.

senescent cells in mice liver, D+Q (MCE Company) were diluted in 100  $\mu$ L 10% polyethylene glycol 400. Mice received the first dose of D+Q (5 mg/kg [D] and 50 mg/kg [Q] body weight) by oral gavage before 3 weeks of CCl<sub>4</sub> injection. D+Q treatment was delivered every 3 weeks for 3 times in total.<sup>26</sup>

### Bile Duct Ligation

To establish liver fibrosis, mice underwent bile duct ligation or sham surgery under anesthesia as described previously.<sup>60</sup> In brief, after midline laparotomy, mice common bile was exposed by a wet cotton swab under sterile conditions and ligated with 1 surgical knot. The sham mice underwent a similar surgical procedure except for the ligation of the bile duct. All mice were killed after 20 days.

### Rapamycin In Vivo Treatment

Rapamycin was applied to inhibit mTOR activation in mice during the establishment of liver fibrosis. Mice received rapamycin (1 mg/kg body weight/day) by intraperitoneal injection daily along with CCl<sub>4</sub> injection until they were killed.<sup>61</sup>

### Patient Samples

Paraffin-embedded, formalin-fixed cirrhotic liver sections were obtained from 6 patients with histologically diagnosed liver cirrhosis confirmed at Nanfang Hospital, Southern Medical University (Guangzhou, China). Serum samples were obtained from age-/sex-matched healthy volunteers and cirrhotic patients. Patient information is presented in Table 1. All of the samples were coded anonymously in accordance with local ethical guidelines, as stipulated by the Declaration of Helsinki, with written informed consent and a protocol approved by the Institutional Review Board of Nanfang Hospital, Southern Medical University.

### Cell Culture

LX-2 cells, an immortalized human HSC line, were gifts from Dr Bai XC of Southern Medical University (Guangzhou, China). Cells were cultured in Dulbecco's modified Eagle medium supplemented with 10% fetal bovine serum, 1% penicillin/streptomycin at 37°C, 5% CO<sub>2</sub>. To observe the effect of MBL on HSC senescence upon liver fibrosis, LX-2 cells were treated with or without 300  $\mu$ mol/L H<sub>2</sub>O<sub>2</sub> and/or 10  $\mu$ g/mL MBL protein purified as we described previously.<sup>30</sup> For p53 inhibition, LX-2 cells were pretreated with 10  $\mu$ mol/L PFT- $\alpha$  ahead of the treatment with H<sub>2</sub>O<sub>2</sub> and/or MBL.<sup>62</sup> For mTOR inhibition, LX-2 cells were exposed to 100 nmol/L rapamycin before the treatment of MBL and/or H<sub>2</sub>O<sub>2</sub>.<sup>63</sup>

### Immunocytochemistry

Paraffin-embedded, formalin-fixed, 5- $\mu$ m-thick tissue sections were processed for immunohistochemical staining with the following primary antibodies: mouse anti-mouse MBL antibody, mouse anti-human MBL antibody, rabbit anti-Ki67 antibody, and rabbit anti- $\alpha$ -SMA antibody. The subsequent procedure followed a method described in previous studies.<sup>15</sup> The expression was visualized by diaminobenzidine staining (Beyotime Biotechnology, Shanghai, China). Sections were lightly counterstained with hematoxylin.

For H&E, Masson, and Sirius Red staining, paraffin-embedded, formalin-fixed, 5- $\mu$ m-thick tissue sections were processed for indicated staining. Five arbitrarily selected fields of 3 random liver sections from 3 to 5 mice per group at 100 $\times$  magnification were analyzed and quantified.

### Immunofluorescence

Paraffin-embedded, formalin-fixed, 5- $\mu$ m-thick tissue sections were processed for immunofluorescent staining with the following primary antibodies: mouse anti-mouse MBL antibody, mouse anti-human MBL antibody, rabbit

**Table 1.** Data From Cirrhotic Patients and Healthy Volunteers

Index	LC	HC
Age, y, means $\pm$ SD	53.55 $\pm$ 9.03	52.35 $\pm$ 9.77
Male/female	23/8	17/3
HBsAg, +/-	26/5	NA
ALT, U/L, means $\pm$ SD	33.22 $\pm$ 13.84	19.1 $\pm$ 8.12
AST, U/L, means $\pm$ SD	39.97 $\pm$ 15.97	24.6 $\pm$ 9.42
Albumin, g/L	31.76 $\pm$ 7.41	40.41 $\pm$ 8.99
TBIL, $\mu$ mol/L	16.62 $\pm$ 8.30	11.46 $\pm$ 3.96
CRP, mg/mL	7.75 $\pm$ 6.24	2.35 $\pm$ 3.02
PT, %	80.89 $\pm$ 16.17	76.28 $\pm$ 16.99
Therapy treatment, resection/TACE/MCT	15/13/3	NA
Child-Pugh, A/B	14/17	NA

CRP, C-reactive protein; HBsAg, hepatitis B surface antigen; HC, healthy control; LC, liver cirrhosis; MCT, microwave coagulation therapy; PT, prothrombin activity; TACE, transcatheter arterial chemoembolization; TBIL, total bilirubin.

anti- $\alpha$ -SMA antibody, rabbit anti-p21 antibody, rabbit anti-Bax antibody, rabbit anti-Bcl2 antibody, rabbit anti-p-H2.X antibody, rabbit anti-p16 antibody, and rabbit anti-CRT antibody. The subsequent procedure followed a method described in our previous study.<sup>13</sup> Sections were mounted with the Mowiol-based antifading medium (Beyotime Biotechnology) and analyzed with a laser scanning microscope system (Nikon Eclipse Ni, Tokyo, Japan). The triple immunofluorescent staining of p53, MBL, and  $\alpha$ -SMA on liver sections was conducted by Servicebio Company (Wuhan, China).

### Quantitative Real-Time PCR

Total RNA was extracted from livers or cells using TRIzol reagent (TransGene Biotech, Beijing, China). Complementary DNA was synthesized from 1  $\mu$ g mRNA using TransScript All-in-One First-Strand Complementary DNA Synthesis Super-Mix (TransGene Biotech) in a total volume of 20  $\mu$ L. Then, the complementary DNA was amplified under the following reaction conditions: denaturation at 94°C, annealing at 55°C, and extension at 72°C for 40 cycles. Real-time PCR was performed with an Eppendorf Realplex PCR system using TransStart Tip Green quantitative reverse-transcription PCR

SuperMix (TransGene Biotech). The expression was normalized to the expression of the housekeeping gene  $\beta$ -actin. The primers used were synthesized in BGI Genomics (Shenzhen, China). The primer sequences used in the experiment are shown in Table 2.

### Immunoblot and Immunoprecipitation

Livers or cells were lysed in cell lysis buffer for Western blot and immunoprecipitation (Beyotime Biotechnology) containing phenylmethanesulfonyl fluoride (Beyotime Biotechnology) on ice for 30 minutes, centrifuged at 14,000  $\times g$  for 15 minutes at 4°C, and the supernatants were collected. Equal amounts of protein from samples were separated by sodium dodecyl sulfate-polyacrylamide gel electrophoresis and transferred onto poly(vinylidene fluoride) membranes (Millipore, Billerica, MA). After incubation with the primary rabbit or mouse antibodies against human MBL, mouse MBL,  $\alpha$ -SMA, p53, p21, mTOR, p-mTOR, AKT, p-AKT, PI3K (p110), Rab8A, CRT, LRP1,  $\beta$ -actin overnight at 4°C, and HRP-conjugated goat anti-rabbit or anti-mouse IgG as the secondary antibody for 1 hour at room temperature. Finally, the membranes were washed 3 times, and detection of the

**Table 2.** Primers for Mice and Human Beings

	Forward primer (5'-3')	Reverse primer (5'-3')
Mouse		
MBL2	TGACAGTGGTTTATGCAGAGAC	CGTCACGTCCATCTTTGCC
p21	CCTGGTGATGTCGACCTG	CCATGAGCGCATCGCAATC
p53	CCGGGGAGTTGTCTTTTCGTG	AATGTGAGGGAAGAGAGTTCCA
MMP2	ACCTGAACACTTTCTATGGCTG	CTTCCGCATGGTCTCGATG
MMP9	GCAGAGGCATACTTGTACCG	TGATGTTATGATGGTCCCACCTG
MMP13	TGTTTGCAGAGCACTACTTGAA	CAGTCACCTCTAAGCCAAAGAAA
IL1 $\beta$	GAAATGCCACCTTTTGACAGTG	TGGATGCTCTCATCAGGACAG
IL6	TACCACTTCACAAGTCGGAGGC	CTGCAAGTGCATCATCGTTGTTCC
IL8	CAAGGCTGGTCCATGCTCC	TGCTATCACTTCCCTTCTGTTGC
CXCL1	ACTGCACCCAAACCGAAGTC	TGGGGACACCTTTTAGCATCTT
CXCL10	CCAAGTGCTGCCGTCATTTTC	GGCTCGCAGGGATGATTTCAA
CCL2	TAAAAACCTGGATCGGAACAAA	GCATTAGCTTCAGATTTACGGGT
CCL5	TTTGCCCTACCTCTCCCTCG	CGACTGCAAGATTGGAGCACT
$\alpha$ -SMA	CCCAGACATCAGGGAGTAATGG	TCTATCGGATACTTCAGCGTCA
Collagen I	GATTCCTGGACCTAAAGGTGC	AGCCTCCTCATCTTTGCCAGCA
Fibronectin1	ATGTGGACCCCTCCTGATAGT	GCCCAGTGATTTTCAGCAAAGG
Timp1	CGAGACCACCTTATACCAGCG	ATGACTGGGGTGTAGGCGTA
$\beta$ -actin	GGCTGTATTCCCCTCCATCG	CCAGTTGGTAAACAATGCCATGT
Human		
p21	TGTCCGTCAGAACCCATGC	AAAGTCGAAGTTCATCGCTC
p53	GAGGTTGGCTCTGACTGTACC	TCCGTCAGTAGATTACCAC
MMP2	AAGTATGGCTTCTGCCCTGA	ATTTGTTGCCAGGAAAGTG
MMP9	CGAACTTTGACAGCGACAAG	CACTGAGGAATGATCTAAGCCC
MMP13	ACTGAGAGGCTCCGAGAAATG	GAACCCCGCATCTTGGCTT
IL1 $\beta$	ATGCACCTGTACGATCACTGA	ACAAGGACATGGAGAACC
IL6	AAAGAGGCACTGGCAGAAAA	TTTACCAGGCAAGTCTCCT
IL8	AAATTTGGGGTGGAAAGGTT	AAGAAACCACCGGAAGGAAC
CXCL1	AACCGAAGTCATAGCCACAC	CCTCCCTTCTGGTCAAGTTG
CCL2	CAGCCAGATGCAATCAATGCC	TGGAATCCTGAACCCACTTCT
$\alpha$ -SMA	CTATGAGGGCTATGCCTTGCC	GCTCAGCAGTAGTAACGAAGGA
Collagen I	CCGGCTCCTGCTCCTTAGCG	CGTTCTGTACGCAGGTGATTGGTGG
Fibronectin 1	AGGAAGCCGAGGTTTAACTG	AGGACGCTCATAAGTGTACC
TIMP1	CAAGATGTATAAGGGTTCCAAGC	TCCATCCTGCAGTTCCTCCAG
$\beta$ -actin	CACCATTGGCAATGAGCGGTTTC	AGGTCTTTGCGGATGTCCACGT

CCL, chemokine (C-C motif) ligand; CXCL, chemokine (C-X-C motif) ligand; IL, interleukin; MMP, matrix metalloproteinase.

target protein was conducted with enhanced chemiluminescence (Thermo Fisher, Carlsbad, CA).

For immunoprecipitation, cell membrane fraction and nonmembrane fraction were incubated with 1  $\mu$ g antibody and protein A/G agarose (Santa Cruz Biotechnology, Santa Cruz, CA) at 4°C overnight, respectively. The eluted immunoprecipitates were resolved via sodium dodecyl sulfate–polyacrylamide gel electrophoresis, and the associations between proteins of interest were examined using specific antibodies.

### Isolation and Culture of Primary Mouse HSCs and Hepatocytes

To extract mice HSCs for mRNA analysis, the fresh liver was perfused slowly via the inferior vena cava with 30 mL warm phosphate-buffered saline at a rate of 5 mL/min, and then digested with 20 mL liver digest medium (RPMI 1640, Collagenase IV at 0.5 mg/mL, and DNase I at 0.1 mg/mL) at a rate of 5 mL/min. After the gall bladder was removed, the livers were carefully excised and passed through a 70- $\mu$ m cell strainer. Then cells were purified by density gradient centrifugation using discontinuous 30%/70% (vol/vol) Percoll (Sigma, St. Louis, MO) gradients. Cells at the upper interface were collected and used for further analysis by quantitative real-time PCR.

To extract and culture mice HSCs, primary HSCs and hepatocytes were extracted from mice livers by collagenase and purified by Percoll as we previously described.<sup>15,64</sup> HSCs and hepatocytes were cultured in Dulbecco's modified Eagle medium supplemented with 10% fetal bovine serum. The activated HSCs were determined by  $\alpha$ -SMA expression. To obtain enough hepatocyte-derived MBL, hepatocytes were stimulated by lipopolysaccharide (100 ng/mL) for 8 hours before medium replacement with fresh culture medium. The supernatants of hepatocytes were collected the next day. Activated HSCs were incubated with these supernatants (30% of total medium) for 48 hours and collected for further experiments.

### AAV-Mediated Hepatic MBL Restoration

For hepatic MBL restoration, the AAV vector expressing mouse MBL under the control of the liver-specific thyroid hormone-binding globulin promoter was generated by Obio Technology (Shanghai, P.R. China). AAV-thyroid hormone-binding globulin (TBG) (pAAV-control) or AAV-TBG-MBL (pAAV-MBL) ( $1 \times 10^{10}$  genome copies/mouse) was delivered by tail-vein injection 3 weeks before the injection of CCl<sub>4</sub>.

### Cell Cycle and Apoptosis Assay

The effect of MBL on cell apoptosis was detected using the cell-cycle staining kit (MultiSciences, Hangzhou, China), according to the manufacturer's instructions. LX-2 cells were seeded into 6-well plates overnight and then cultured in the media with the indicated concentration of MBL and/or H<sub>2</sub>O<sub>2</sub> for 48 hours. Subsequently, the cells were collected and resuspended in 1 mL DNA staining solution and 10  $\mu$ L permeabilization solution for 30 minutes in the dark. Data

were acquired on a LSRII/Fortessa flow cytometer (BD Biosciences, Heidelberg, Germany) and analyzed using FlowJo software (Tree Star, Ashland, OR).

The effect of MBL on cell apoptosis was detected using the Annexin-V/7-AAD kit (MultiSciences), according to the manufacturer's instructions. LX-2 cells were seeded into 6-well plates overnight and then cultured in the media with the indicated concentration of MBL and/or H<sub>2</sub>O<sub>2</sub> for 48 hours. Subsequently, the cells were collected and resuspended in 100  $\mu$ L Binding Buffer containing 5  $\mu$ L Annexin-V and 10  $\mu$ L 7-AAD for 15 minutes in the dark. Data were acquired on a LSRII/Fortessa flow cytometer (BD Biosciences) and analyzed using FlowJo software.

### ELISA Assay

To measure serum levels of MBL, ALT, AST, and LDH, serums were collected from human patients or mice. The serum levels of MBL in patients and ALT, AST, and LDH in mice were measured by ELISA. The assay kits for mouse ALT, mouse AST, and mouse lactate dehydrogenase were purchased from Jiancheng Biotech (Nanjing, China) and a kit for human MBL from R&D Systems.

### Senescence-Associated $\beta$ -Galactosidase Staining

The effect of MBL on senescence was detected using the senescent-associated  $\beta$ -galactosidase staining kit (Beyotime Biotechnology) according to the manufacturer's instructions. Cells seeded on 6-well plates or paraffin-embedded, formalin-fixed, 5- $\mu$ m-thick tissue sections were incubated with a combination of staining solution overnight. Five random fields from each section were analyzed under a magnification of 100 $\times$ , 3 random sections from each mouse were analyzed, and data from 3 to 5 mice per group were used to compare different treatment groups.

### Statistical Analysis

All values are expressed as means  $\pm$  SEM. Unpaired Student *t* test or 1-way analysis of variance followed by the Tukey post hoc tests was used for multiple group comparisons. *P* < .05 was considered significant. Statistics were calculated with GraphPad Prism version 8 (GraphPad Software, San Diego, CA).

### References

1. Parola M, Pinzani M. Liver fibrosis: pathophysiology, pathogenetic targets and clinical issues. *Mol Aspects Med* 2019;65:37–55.
2. Moon AM, Singal AG, Tapper EB. Contemporary epidemiology of chronic liver disease and cirrhosis. *Clin Gastroenterol Hepatol* 2020;18:2650–2666.
3. Marrone G, Shah VH, Gracia-Sancho J. Sinusoidal communication in liver fibrosis and regeneration. *J Hepatol* 2016;65:608–617.
4. Higashi T, Friedman SL, Hoshida Y. Hepatic stellate cells as key target in liver fibrosis. *Adv Drug Deliv Rev* 2017; 121:27–42.

5. Nishizawa H, Iguchi G, Fukuoka H, Takahashi M, Suda K, Bando H, Matsumoto R, Yoshida K, Otake Y, Ogawa W, Takahashi Y. IGF-I induces senescence of hepatic stellate cells and limits fibrosis in a p53-dependent manner. *Sci Rep* 2016;6:34605.
6. Panebianco C, Oben JA, Vinciguerra M, Paziienza V. Senescence in hepatic stellate cells as a mechanism of liver fibrosis reversal: a putative synergy between retinoic acid and PPAR-gamma signalings. *Clin Exp Med* 2017; 17:269–280.
7. Kisseleva T, Brenner D. Molecular and cellular mechanisms of liver fibrosis and its regression. *Nat Rev Gastroenterol Hepatol* 2021;18:151–166.
8. Cai X, Wang J, Wang J, Zhou Q, Yang B, He Q, Weng Q. Intercellular crosstalk of hepatic stellate cells in liver fibrosis: new insights into therapy. *Pharmacol Res* 2020; 155:104720.
9. de Oliveira da Silva B, Ramos LF, Moraes KCM. Molecular interplays in hepatic stellate cells: apoptosis, senescence, and phenotype reversion as cellular connections that modulate liver fibrosis. *Cell Biol Int* 2017; 41:946–959.
10. Ip WK, Takahashi K, Ezekowitz RA, Stuart LM. Mannose-binding lectin and innate immunity. *Immunol Rev* 2009; 230:9–21.
11. Wagner S, Lynch NJ, Walter W, Schwaeble WJ, Loos M. Differential expression of the murine mannose-binding lectins A and C in lymphoid and nonlymphoid organs and tissues. *J Immunol* 2003;170:1462–1465.
12. Rakhshandehroo M, Stienstra R, de Wit NJ, Bragt MC, Haluzik M, Mensink RP, Muller M, Kersten S. Plasma mannose-binding lectin is stimulated by PPARalpha in humans. *Am J Physiol Endocrinol Metab* 2012; 302:E595–E602.
13. van Asbeck EC, Hoepelman AI, Scharringa J, Herpers BL, Verhoef J. Mannose binding lectin plays a crucial role in innate immunity against yeast by enhanced complement activation and enhanced uptake of polymorphonuclear cells. *BMC Microbiol* 2008;8:229.
14. Sastry R, Wang JS, Brown DC, Ezekowitz RA, Tauber AI, Sastry KN. Characterization of murine mannose-binding protein genes Mbl1 and Mbl2 reveals features common to other collectin genes. *Mamm Genome* 1995; 6:103–110.
15. Li J, Li H, Yu Y, Liu Y, Liu Y, Ma Q, Zhang L, Lu X, Wang XY, Chen Z, Zuo D, Zhou J. Mannan-binding lectin suppresses growth of hepatocellular carcinoma by regulating hepatic stellate cell activation via the ERK/COX-2/PGE2 pathway. *Oncoimmunology* 2019;8: e1527650.
16. Cai Y, Zhang W, Xiong S. Mannose-binding lectin blunts macrophage polarization and ameliorates lupus nephritis. *PLoS One* 2013;8:e62465.
17. Wong C, Jayaram L, Chang L. Mannose-binding lectin and innate immunity in bronchiectasis. *Lancet Respir Med* 2013;1:179–180.
18. Glargaard S, Boysen T, Pilely K, Garred P, Ytting H. Prognostic value of lectin pathway molecules and complement proteins in ascitic fluid and blood in patients with liver cirrhosis. *Scand J Gastroenterol* 2018; 53:64–69.
19. Koutsounaki E, Goulielmos GN, Koulentaki M, Choulaki C, Kouroumalis E, Galanakis E. Mannose-binding lectin MBL2 gene polymorphisms and outcome of hepatitis C virus-infected patients. *J Clin Immunol* 2008;28:495–500.
20. Huang YH, Chen MH, Guo QL, Chen ZX, Chen QD, Wang XZ. Interleukin-10 induces senescence of activated hepatic stellate cells via STAT3-p53 pathway to attenuate liver fibrosis. *Cell Signal* 2020;66:109445.
21. Jung SH, Hwang HJ, Kang D, Park HA, Lee HC, Jeong D, Lee K, Park HJ, Ko YG, Lee JS. mTOR kinase leads to PTEN-loss-induced cellular senescence by phosphorylating p53. *Oncogene* 2019;38:1639–1650.
22. Zhang CY, Yuan WG, He P, Lei JH, Wang CX. Liver fibrosis and hepatic stellate cells: etiology, pathological hallmarks and therapeutic targets. *World J Gastroenterol* 2016;22:10512–10522.
23. Krizhanovsky V, Yon M, Dickins RA, Hearn S, Simon J, Miething C, Yee H, Zender L, Lowe SW. Senescence of activated stellate cells limits liver fibrosis. *Cell* 2008; 134:657–667.
24. Schnabl B, Purbeck CA, Choi YH, Hagedorn CH, Brenner D. Replicative senescence of activated human hepatic stellate cells is accompanied by a pronounced inflammatory but less fibrogenic phenotype. *Hepatology* 2003;37:653–664.
25. Xu M, Pirtskhalava T, Farr JN, Weigand BM, Palmer AK, Weivoda MM, Inman CL, Ogradnik MB, Hachfeld CM, Fraser DG, Onken JL, Johnson KO, Verzosa GC, Langhi LGP, Weigl M, Giorgadze N, LeBrasseur NK, Miller JD, Jurk D, Singh RJ, Allison DB, Ejima K, Hubbard GB, Ikeno Y, Cubro H, Garovic VD, Hou X, Weroha SJ, Robbins PD, Niedernhofer LJ, Khosla S, Tchkonja T, Kirkland JL. Senolytics improve physical function and increase lifespan in old age. *Nat Med* 2018; 24:1246–1256.
26. Li F, Huangyang P, Burrows M, Guo K, Riscal R, Godfrey J, Lee KE, Lin N, Lee P, Blair IA, Keith B, Li B, Simon MC. FBP1 loss disrupts liver metabolism and promotes tumorigenesis through a hepatic stellate cell senescence secretome. *Nat Cell Biol* 2020;22:728–739.
27. Luo X, Jiang X, Li J, Bai Y, Li Z, Wei P, Sun S, Liang Y, Han S, Li X, Zhang B. Insulin-like growth factor-1 attenuates oxidative stress-induced hepatocyte premature senescence in liver fibrogenesis via regulating nuclear p53-progerin interaction. *Cell Death Dis* 2019;10:451.
28. Jin H, Lian N, Zhang F, Chen L, Chen Q, Lu C, Bian M, Shao J, Wu L, Zheng S. Activation of PPARgamma/P53 signaling is required for curcumin to induce hepatic stellate cell senescence. *Cell Death Dis* 2016;7:e2189.
29. Bernard M, Yang B, Migneault F, Turgeon J, Dieude M, Olivier MA, Cardin GB, El-Diwanly M, Underwood K, Rodier F, Hebert MJ. Autophagy drives fibroblast senescence through MTORC2 regulation. *Autophagy* 2020;16:2004–2016.
30. Zhao N, Wu J, Xiong SM, Zhang LY, Lu X, Chen SL, Wu QF, Wang HL, Liu Y, Chen ZL, Zuo DM. Mannan-

- binding lectin, a serum collectin, suppresses T-cell proliferation via direct interaction with cell surface calreticulin and inhibition of proximal T-cell receptor signaling. *FASEB J* 2017;31:2405–2417.
31. Park KS, Sin PJ, Lee DH, Cha SK, Kim MJ, Kim NH, Baik SK, Jeong SW, Kong ID. Switching-on of serotonergic calcium signaling in activated hepatic stellate cells. *World J Gastroenterol* 2011;17:164–173.
  32. Pallero MA, Elzie CA, Chen J, Mosher DF, Murphy-Ullrich JE. Thrombospondin 1 binding to calreticulin-LRP1 signals resistance to anoikis. *FASEB J* 2008;22:3968–3979.
  33. Luo L, Wall AA, Tong SJ, Hung Y, Xiao Z, Tarique AA, Sly PD, Fantino E, Marzolo MP, Stow JL. TLR crosstalk activates LRP1 to recruit Rab8a and PI3Kgamma for suppression of inflammatory responses. *Cell Rep* 2018;24:3033–3044.
  34. Choteau L, Parny M, Francois N, Bertin B, Fumery M, Dubuquoy L, Takahashi K, Colombel JF, Jouault T, Poulain D, Sendid B, Jawhara S. Role of mannose-binding lectin in intestinal homeostasis and fungal elimination. *Mucosal Immunol* 2016;9:767–776.
  35. Vasta GR, Quesenberry M, Ahmed H, O'Leary N. C-type lectins and galectins mediate innate and adaptive immune functions: their roles in the complement activation pathway. *Dev Comp Immunol* 1999;23:401–420.
  36. Ji X, Gewurz H, Spear GT. Mannose binding lectin (MBL) and HIV. *Mol Immunol* 2005;42:145–152.
  37. Ehltling C, Wolf SD, Bode JG. Acute-phase protein synthesis: a key feature of innate immune functions of the liver. *Biol Chem* 2021;402:1129–1145.
  38. Moshage H. Cytokines and the hepatic acute phase response. *J Pathol* 1997;181:257–266.
  39. Sorensen CM, Hansen TK, Steffensen R, Jensenius JC, Thiel S. Hormonal regulation of mannan-binding lectin synthesis in hepatocytes. *Clin Exp Immunol* 2006;145:173–182.
  40. Gupta B, Raghav SK, Das HR. S-nitrosylation of mannose binding lectin regulates its functional activities and the formation of autoantibody in rheumatoid arthritis. *Nitric Oxide* 2008;18:266–273.
  41. Bouwman LH, Roos A, Terpstra OT, de Knijff P, van Hoek B, Verspaget HW, Berger SP, Daha MR, Frolich M, van der Sliik AR, Doxiadis II, Roep BO, Schaapherder AF. Mannose binding lectin gene polymorphisms confer a major risk for severe infections after liver transplantation. *Gastroenterology* 2005;129:408–414.
  42. Wells RG, Schwabe RF. Origin and function of myofibroblasts in the liver. *Semin Liver Dis* 2015;35:e1.
  43. Mederacke I, Hsu CC, Troeger JS, Huebener P, Mu X, Dapito DH, Pradere JP, Schwabe RF. Fate tracing reveals hepatic stellate cells as dominant contributors to liver fibrosis independent of its aetiology. *Nat Commun* 2013;4:2823.
  44. Bataller R, Brenner DA. Liver fibrosis. *J Clin Invest* 2005;115:209–218.
  45. Schrader J, Fallowfield J, Iredale JP. Senescence of activated stellate cells: not just early retirement. *Hepatology* 2009;49:1045–1047.
  46. Aravinthan AD, Alexander GJM. Senescence in chronic liver disease: is the future in aging? *J Hepatol* 2016;65:825–834.
  47. Song P, Zhao Q, Zou MH. Targeting senescent cells to attenuate cardiovascular disease progression. *Ageing Res Rev* 2020;60:101072.
  48. Alsuraih M, O'Hara SP, Woodrum JE, Pirius NE, LaRusso NF. Genetic or pharmacological reduction of cholangiocyte senescence improves inflammation and fibrosis in the Mdr2 (-/-) mouse. *JHEP Rep* 2021;3:100250.
  49. Popov Y, Patsenker E, Fickert P, Trauner M, Schuppan D. Mdr2 (Abcb4)-/- mice spontaneously develop severe biliary fibrosis via massive dysregulation of pro- and antifibrogenic genes. *J Hepatol* 2005;43:1045–1054.
  50. Scholten D, Trebicka J, Liedtke C, Weiskirchen R. The carbon tetrachloride model in mice. *Lab Anim* 2015;49:4–11.
  51. Kim YO, Popov Y, Schuppan D. Optimized mouse models for liver fibrosis. *Methods Mol Biol* 2017;1559:279–296.
  52. Kirkland JL, Tchkonja T. Senolytic drugs: from discovery to translation. *J Intern Med* 2020;288:518–536.
  53. Elsallabi O, Patruno A, Pesce M, Cataldi A, Carradori S, Gallorini M. Fisetin as a senotherapeutic agent: biopharmaceutical properties and crosstalk between cell senescence and neuroprotection. *Molecules* 2022;27:738.
  54. Schwabe RF, Tabas I, Pajvani UB. Mechanisms of fibrosis development in nonalcoholic steatohepatitis. *Gastroenterology* 2020;158:1913–1928.
  55. Khor ES, Wong PF. The roles of MTOR and miRNAs in endothelial cell senescence. *Biogerontology* 2020;21:517–530.
  56. Qin YN, Zhong YG, Yang GL, Ma TR, Jia LY, Huang C, Li Z. Profiling of concanavalin A-binding glycoproteins in human hepatic stellate cells activated with transforming growth factor-beta 1. *Molecules* 2014;19:19845–19867.
  57. Duus K, Thielens NM, Lacroix M, Tacnet P, Frachet P, Holmskov U, Houen G. CD91 interacts with mannan-binding lectin (MBL) through the MBL-associated serine protease-binding site. *FEBS J* 2010;277:4956–4964.
  58. Kang LI, Isse K, Koral K, Bowen WC, Muratoglu S, Strickland DK, Michalopoulos GK, Mars WM. Tissue-type plasminogen activator suppresses activated stellate cells through low-density lipoprotein receptor-related protein 1. *Lab Invest* 2015;95:1117–1129.
  59. Barcena-Varela M, Paish H, Alvarez L, Uriarte I, Latasa MU, Santamaria E, Recalde M, Garate M, Claveria A, Colyn L, Arechederra M, Iraburu MJ, Milkiewicz M, Milkiewicz P, Sangro B, Robinson SM, French J, Pardo-Saganta A, Oyarzabal J, Prosper F, Rombouts K, Oakley F, Mann J, Berasain C, Avila MA, M GF-B. Epigenetic mechanisms and metabolic reprogramming in fibrogenesis: dual targeting of G9a and DNMT1 for the inhibition of liver fibrosis. *Gut* 2021;70:388–400.



60. Tag CG, Sauer-Lehnen S, Weiskirchen S, Borkham-Kamphorst E, Tolba RH, Tacke F, Weiskirchen R. Bile duct ligation in mice: induction of inflammatory liver injury and fibrosis by obstructive cholestasis. *J Vis Exp* 2015;10:52438.
61. Shan L, Ding Y, Fu Y, Zhou L, Dong X, Chen S, Wu H, Nai W, Zheng H, Xu W, Bai X, Jia C, Dai M. mTOR overactivation in mesenchymal cells aggravates CCl4-induced liver fibrosis. *Sci Rep* 2016;6:36037.
62. Jia F, Wu Q, Wang Z, Zhang M, Yuan S, Che Y, Li B, Hu Z, Hu X. BOP1 Knockdown attenuates neointimal hyperplasia by activating p53 and inhibiting nascent protein synthesis. *Oxid Med Cell Longev* 2021;2021:5986260.
63. Salazar G, Cullen A, Huang J, Zhao Y, Serino A, Hilenski L, Patrushev N, Forouzandeh F, Hwang HS. SQSTM1/p62 and PPARGC1A/PGC-1alpha at the interface of autophagy and vascular senescence. *Autophagy* 2020;16:1092–1110.
64. Chen Y, Hu M, Deng F, Wang P, Lin J, Zheng Z, Liu Y, Dong L, Lu X, Chen Z, Zhou J, Zuo D. Mannan-binding lectin deficiency augments hepatic endoplasmic reticulum stress through IP3R-controlled calcium release. *Cell Calcium* 2021;100:102477.

Medical University, Guangzhou, Guangdong, 510515 China. e-mail: [zdaming@smu.edu.cn](mailto:zdaming@smu.edu.cn); fax: (86) 20-61648221. Jia Zhou, MD, PhD, Department of Immunology, School of Basic Medical Sciences, Southern Medical University, Guangzhou, Guangdong, 510515 China. e-mail: [yuguomm@smu.edu.cn](mailto:yuguomm@smu.edu.cn); fax: (86) 20-61648221.

#### CRedit Authorship Contributions

Feng-Kun Zhang (Data curation: Lead; Methodology: Lead; Software: Lead; Visualization: Lead; Writing – original draft: Lead)  
 Qian-Zhi Ni (Investigation: Equal)  
 Kang Wang (Methodology: Supporting)  
 Hui-Jun Cao (Investigation: Supporting)  
 Dongxian Guan (Methodology: Equal)  
 Er-Bin Zhang (Data curation: Supporting)  
 Ning Ma (Formal analysis: Supporting)  
 Yi-Kang Wang (Methodology: Supporting)  
 Qian-Wen Zheng (Resources: Supporting)  
 Sheng Xu (Software: Supporting)  
 Bing Zhu (Validation: Supporting)  
 Tian-Wei Chen (Software: Supporting)  
 Ji Xia (Resources: Supporting)  
 Xiao-Song Qiu (Software: Supporting)  
 Xu-Fen Ding (Validation: Supporting)  
 Hao Jiang (Investigation: Supporting)  
 Lin Qiu (Software: Supporting)  
 Xiang Wang (Visualization: Supporting)  
 Wei Chen (Resources: Supporting)  
 Shu-Qun Cheng (Supervision: Supporting)  
 Dong Xie (Conceptualization: Lead; Funding acquisition: Lead)  
 Jingjing Li, PhD (Conceptualization: Lead; Funding acquisition: Lead; Supervision: Lead)

#### Conflicts of interest

The authors disclose no conflicts.

#### Funding

This work was supported in part by the National Natural Science Foundation of China (81971550, 81873872, 82071781 and 82171745), Science and Technology Planning Project of Guangzhou (202002030160), and Guangdong Basic and Applied Basic Research Foundation of Guangdong Province (2022A1515012437).

---

Received August 15, 2021. Accepted March 28, 2022.

#### Correspondence

Address correspondence to: Daming Zuo, MD, PhD, Department of Medical Laboratory, School of Laboratory Medicine and Biotechnology, Southern